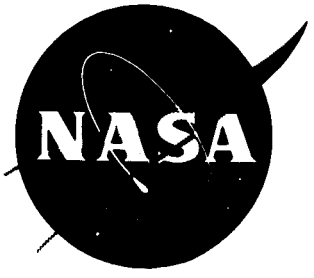

TECHNICAL NOTE
D-49

SOME ASPECTS OF AIR-HELIUM SIMULATION AND HYPERSONIC APPROXIMATIONS

By Eugene S. Love, Arthur Henderson, Jr.,
and Mitchel H. Bertram

Langley Research Center
Langley Field, Va.

NATIONAL AERONAUTICS AND SPACE ADMINISTRATION

WASHINGTON

October 1959

1J

CONTENTS

NATIONAL AERONAUTICS AND SPACE ADMINISTRATION

TECHNICAL NOTE D-49

SOME ASPECTS OF AIR-HELIUM SIMULATION AND HYPERSONIC APPROXIMATIONS

By Eugene S. Love, Arthur Henderson, Jr.,
and Mitchel H. Bertram

SUMMARY

Some illustrations of the differences that may be expected between results obtained in hypersonic wind tunnels that employ air and results obtained in those that employ helium as the test medium (imperfect-gas effects are not considered) are compiled and presented herein. Simple expressions are presented that demonstrate the possibility of simulating air results in helium tests and of transforming helium data to equivalent air data. Nonviscous and viscous simulations are considered. In most cases, the methods and the general forms of the expressions for simulation that are derived are applicable to any two ideal gases having different ratios of specific heats.

INTRODUCTION

The significant contributions that hypersonic helium tunnels can make in the study of fluid-dynamic problems is well recognized, and much information has been published that deals with hypersonic tests in helium or with supporting information. References 1 to 18 are some examples of this work. Most of the reasons for resorting to the use of helium in hypersonic tunnels have been discussed in the literature and will not be reviewed in detail here. Briefly, the primary advantages of helium over air as a test medium in hypersonic tunnels are the much lower pressure ratios required for tunnel operation, the more attractive area ratios (from the viewpoint of throat design), the inertness of helium, the higher Reynolds numbers and dynamic pressures obtainable, and, probably above all else, the very low liquefaction point of helium.[1] This low liquefaction point virtually eliminates the need for heaters in helium hypersonic tunnels until Mach numbers of the order of 26 are exceeded, as illustrated in figure 1. For Mach numbers of the order of 40 a heater capable of

[1]Helium is the most difficult of all gases to liquefy; its critical temperature is about 9.4° R. See reference 15 for additional information on helium.

producing a stagnation temperature of the order of 1,000° R appears adequate to avoid liquefaction.

There are, of course, basic differences between air and helium that cause concern when hypersonic tests are undertaken in helium with a view toward interpreting the results in terms of what might occur in air. For many purely fluid-dynamic studies this simulation problem is of no concern; however, for some fluid-dynamic studies and for all aerodynamic studies it is important to know whether adequate air-helium simulation can be achieved, or whether helium data can be suitably transformed to air data. It appears reasonably certain that simulation of the imperfect-gas effects that become significant at extremes of temperature and pressure is impossible. However, for a wide range of test conditions an ideal gas may be assumed, and for this case the primary source of the simulation problem lies in the difference in the ratio of specific heats for helium and air, 5/3 and 7/5, respectively; in this case there is some opportunity for simulation.

A number of aspects of the air-helium simulation problem have been examined recently as part of a study of the possible utilization of a hypersonic helium tunnel and the interpretation of results of tests therein. An ideal gas has been assumed throughout. It is the purpose of this paper to compile these examinations and to present them with the belief that, in spite of the random nature of the subjects considered, the results may be of interest to those who are conducting hypersonic studies in helium or are concerned with the simulation conditions for two gases with different ratios of specific heat. The discussion is in two parts; the first part deals with inviscid flow and the second part with viscous flow.[2]

In some of the results that are presented, more significant figures have been retained in the value of a parameter than is warranted by the accuracies of the approximations. In such cases the intent is to bring out certain aspects that might otherwise be obscured; for example, one is to show that the variation of a parameter with a variable occurs smoothly.

SYMBOLS

A,B	constants in equation (119)
a	half height of body

[2]Subsequent to the completion of this paper, the book "Hypersonic Flow Theory" by Wallace D. Hayes and Ronald F. Probstein was published by Academic Press, Inc. (New York), and is now available. This work includes results similar to some of the results presented herein and affords several additional comparisons of air and helium, as well as some discussions of γ effects and hypersonic approximations that are pertinent to the contents of this paper.

C	linear viscosity coefficient
C_D	drag coefficient
C_F	average skin-friction coefficient
C_L	lift coefficient
C_N	normal-force coefficient
C_p	pressure coefficient
c	chord
D	diameter
d	detachment distance
g	constant in equation (119)
K	similarity parameter, $M_1\delta$ or $M_1\,\Delta v$
K_i	constant in incompressible skin-friction laws
k	density ratio across bow shock, ρ_1/ρ_2
L/D	lift-drag ratio
l	length measured from leading edge
M	Mach number
$m \equiv \dfrac{\rho_l u_l}{\sqrt{p_{max}\rho_{max}}}$	
$\tilde{m}_1 \equiv \dfrac{\rho_l u_l}{\rho_1 u_1}$	
N	Reynolds number exponent in incompressible skin-friction laws
N_{Kn}	Knudsen number
N_{Pr}	Prandtl number

N_ν molecular speed ratio

p static pressure

p_t stagnation pressure

$\Delta p = p - p_1$

q dynamic pressure

R Reynolds number, based on free-stream condition unless otherwise specified

r radius of curvature of nose

r_s radius of curvature of shock at axis

S area

T temperature

T^* reference temperature

t leading-edge thickness

$$U \equiv r \frac{du}{dx}\left(\frac{p_{max}}{\rho_{max}}\right)^{-1/2}$$

$$U_1 \equiv \frac{r}{u_1}\frac{du}{dx}$$

$$\tilde{U} \equiv \frac{D}{u_2}\frac{du}{dx}$$

$$\tilde{U}_1 \equiv \frac{D}{u_1}\frac{du}{dx}$$

u local velocity

V velocity

W weight

x distance parallel to body surface

y distance normal to free-stream direction and measured from plane of symmetry

$Z \equiv \frac{M_1\sqrt{C}}{\sqrt{R}}$

α angle of attack

β Sutherland's constant

γ ratio of specific heats

$\Delta\nu$ expansion angle

δ two-dimensional turning through an oblique shock, or flow deflection angle

δ_e flow deflection angle at edge of boundary layer

δ^* displacement thickness of boundary layer

ϵ shock-wave angle

θ seminose angle

Λ sweepback angle

μ viscosity

μ^* viscosity corresponding to T^*

ρ density

$\sigma \equiv \frac{C_{F,H}}{C_{F,A}}$ for $R_H = R_A$

$\varphi \equiv 90^\circ - \delta$

$\bar{\chi} \equiv \frac{M_1^3\sqrt{C}}{\sqrt{R}}$

$\psi = \delta \tan \Lambda$

ω exponent in power form of viscosity law

Subscripts:

1 free stream

2	behind shock, or local conditions
A	in air
detach	detachment
f	final value after Prandtl-Meyer expansion
H	in helium
i	incompressible
l	local inviscid condition
max	maximum value

A prime indicates the sonic point.

DISCUSSION

Inviscid Flow

Preliminary considerations.- Although there is general agreement that the so-called Newtonian simulation argument is more paradoxical than conclusive, it occurs so often in discussions of air-helium simulation problems that some mention of it appears to be in order before discussing the effect of the ratio of specific heats.

The Newtonian simulation argument stems from the fact that the simple Newtonian theory for predicting the pressure coefficient at hypersonic speeds, that is,

$$C_p = 2 \sin^2\delta \tag{1}$$

has within certain limits of application shown sufficient agreement with experimental results in air to receive general acceptance. As is well known, this expression can be developed either by setting $\gamma = 1$ and $M_1 = \infty$ in the exact shock equations or by mass impact considerations. Since this latter method does not involve γ, the interpretation leading to the Newtonian argument is that equation (1) is independent of γ effects and, thus, that if it is satisfactory for even restricted use in air, which it seems to be, then it should be satisfactory within the same restrictions for all values of γ, not only $\gamma = 7/5$. Hence, the Newtonian simulation argument is that the effects of γ on the pressure coefficient are negligible for all conditions where Newtonian theory has given satisfactory results in air and, consequently, that for these conditions simulation is not a problem when gases having different values of γ are used.

Although this argument has some merit, it is difficult to accept without reservation. Basic factors such as the effects of γ on the accuracy of hypersonic approximations, examples of which will be given in the following section, are sufficient cause to examine further the effect of γ in the air-helium simulation problem.

Examples of effects of γ on accuracy of hypersonic approximations.- In reference 19 the effect of γ upon the accuracy of the predictions of several hypersonic approximations has been examined for the case of $K \to \infty$, where K is the hypersonic similarity parameter $M_1\delta$. The predicted quantity in this examination is the limiting value of the initial pressure gradient on plane and axisymmetric ogives. The approximations include the tangent-wedge and tangent-cone, Newtonian, and shock-expansion approximations. The results for the plane ogive show (ref. 19) that for $\gamma = 5/3$ all the approximations give good predictions of the limiting value of the initial pressure gradient and have the same order of accuracy. As γ decreases from $5/3$ to 1 the tangent-wedge and shock-expansion approximations become less accurate and introduce significant errors below γ of the order of $7/5$. The tangent-wedge second-order approximation and the Newtonian-plus-centrifugal-force approximation give good results for all values of γ in the range $1 \leq \gamma \leq 5/3$. For the axisymmetric ogive the limiting value of the initial pressure gradient is predicted very accurately by the Newtonian-plus-centrifugal-force approximation for all values of γ in the range $1 \leq \gamma \leq 5/3$. For $\gamma = 5/3$, the shock-expansion approximation gives good results and the tangent-cone approximation gives fair results; but, as occurs for the plane ogive, these approximations become less accurate with decreasing values of γ and experience significant errors below values of γ of about $7/5$.

The excellent predictions by the shock-expansion method at large values of γ and the poor predictions at small values of γ arise because a high order of accuracy for this method requires that the expansion waves generated at the body surface be almost entirely absorbed by the shock wave. In reference 20, this was shown to occur for $\gamma = 7/5$ up to values of δ near those producing shock detachment, and subsequently in reference 4 it was shown to occur to an even greater degree for $\gamma = 5/3$. This improvement with increasing γ is compatible with the explanation given in reference 19 for the inaccuracy of the method as $\gamma \to 1$; that is, as $\gamma \to 1$ the reflected waves from the shock become nearly as strong as the expansion waves from the body.

The foregoing results show sufficiently large effects of γ upon the accuracy of hypersonic approximations to warrant an examination of the effect of γ upon the pressure coefficient given by certain approximations for the simple case of an inclined flat plate. First, consider the Newtonian approximation, equation (1), at $M_1 = \infty$ where it should

best apply. A comparison of Newtonian theory with the exact theory is shown in figures 2(a) to 2(d) for $M_1 = \infty$ and for values of γ of 1, 6/5, 7/5, and 5/3. As γ increases from 1, where Newtonian theory is exact, this comparison shows Newtonian theory to become increasingly inaccurate ($\delta \ll 1$ excluded). For example, as γ increases from 1 to 5/3, an accurate prediction would require the constant in Newtonian theory to increase from 2 to about 2.7, or about 35 percent. This significant error in the use of Newtonian theory at large values of γ for inclined flat plates is in marked contrast to the success of Newtonian theory for the slender axisymmetric surface, for which reference 19 has shown that the same increase in γ would require the constant in Newtonian theory to increase from 2 to about 2.1, or only about 5 percent. Thus, when γ deviates appreciably from unity, Newtonian theory experiences considerably less error in applications to cones and slender bodies of revolution than to two-dimensional surfaces. For gases with large values of γ, such as air and helium, the previously mentioned Newtonian simulation argument is therefore seen to be restricted to slender bodies of revolution, for which it may be reasonably appropriate.

Some of the reasons for the inaccuracies that have been shown for Newtonian theory lie in the implication of this theory that the shock wave is coincident with the body surface, that is, $(\epsilon - \delta) = 0$. For both cones and wedges, for $K \gg 1$ it may be shown that $(\epsilon - \delta) \approx (\text{Constant})\delta(\gamma - 1)$ where the constant of proportionality is 1/2 for wedges and 1/4 for cones. Thus, the greater the value of γ the less the Newtonian condition of $(\epsilon - \delta) = 0$ is satisfied. This condition is also more nearly satisfied by cones than by wedges in that the value of $(\epsilon - \delta)$ for cones is indicated to be one-half that for wedges.

Consider next the tangent-wedge approximation. For large values of M_1 and small to moderate values of δ, the shock equations may be simplified to yield (as in ref. 19, e.g.)

$$C_{p,2} = 2\delta^2\left[\frac{\gamma + 1}{4} + \sqrt{\left(\frac{\gamma + 1}{4}\right)^2 + \frac{1}{K^2}}\right] \tag{2}$$

This approximation is known to give values of $C_{p,2}$ that agree closely with the exact values. For $K \gg 1$, the tangent-wedge approximation reduces to

$$C_{p,2} = \delta^2(\gamma + 1) \tag{3}$$

Since this approximation should also give the best predictions at $K = \infty$, it is of interest to consider first the accuracy for the ideal condition of $M_1 = \infty$. Accordingly, curves given by this approximation are also shown in figure 2. The values of δ and $C_{p,2}$ for detachment at $M_1 = \infty$ are shown in the figure and are given by the approximations

$$\delta_{detach} = \tan^{-1} \frac{1}{\sqrt{\gamma^2 - 1}} \tag{4}$$

and

$$(C_{p,2})_{detach} = \frac{2}{\gamma} \tag{5}$$

which are exact for $M_1 = \infty$. Comparison of the tangent-wedge prediction with the exact curve shows that this prediction is notably poor at $\gamma = 1$ for other than small values of δ but improves with increasing values of γ and excels the Newtonian prediction as γ exceeds the order of 6/5. The improvement with increasing values of γ is shown in figure 3 in the form of percent error. The very small errors at low values of δ are compatible with the assumptions under which the approximation is derived. For $\gamma = 7/5$ (air) and $\gamma = 5/3$ (helium) the errors are not large even near shock detachment.

The deficiency of the tangent-wedge approximation at $\gamma = 1$ and $M_1 = \infty$ can be eliminated completely if δ^2 is replaced by $\sin^2\delta$. This obvious modification, coupled with the form of Newtonian theory, gives rise to the observation in the literature that in the limit of $\gamma = 1$ and $M_1 = \infty$ Newtonian theory may also be expressed as

$$C_{p,2} = (\gamma + 1)\sin^2\delta \tag{6}$$

and that this expression is in close agreement with exact theory for $\gamma = 7/5$ and $M_1 \gg 1$. (See, e.g., ref. 21.)

The preceding examinations in this paper imply that equation (6) may be quite useful for $1 \leqq \gamma \leqq 5/3$ for as shown in the discussion of Newtonian theory, the value of $C_{p,2}/\sin^2\delta$ in this application must vary appreciably with γ; the results given in figure 2 for tangent-wedge theory and Newtonian theory imply, in relation to exact theory, that the desired variation of $C_{p,2}/\sin^2\delta$ is, at least for $M_1 = \infty$, closely approximated by the tangent-wedge variation of $(\gamma + 1)$. Equation (6) may thus be

regarded as a modification of either Newtonian or tangent-wedge theory; it will be referred to herein as flat-plate-modified Newtonian theory to associate it with, and at the same time distinguish it from, blunt-nose-modified Newtonian theory to be discussed in a subsequent section. It should not be used to predict pressures on a blunt nose or for values of δ beyond those producing shock detachment. In this regard, blunt-nose-modified Newtonian theory should not be used to predict pressures on inclined flat plates until values of δ near those producing shock detachment are exceeded.

The predictions given by equation (6), again under the ideal condition of $M_1 = \infty$, are shown in figure 2 for comparison with the other results, and the percent error is shown in figure 4. The predictions of equation (6) experience a small loss in accuracy with increasing values of γ, but the errors, in general, remain small except very near shock detachment for $\gamma = 5/3$.

Thus, in the ideal limit of $M_1 = \infty$, equation (6) gives better predictions than equation (3) except for values of δ within about 7° of shock detachment for $\gamma = 5/3$. If the term $\frac{\gamma - 1}{\gamma + 1} \sin^4\delta$ is added to the right-hand side of equation (6), the predictions are in essential agreement with exact theory, except near shock detachment when $\gamma > 1$.

For the Mach number range in which most of the published experimental work in helium has been done (i.e., $M_1 \approx 20$) the relative positions of the curves and the values of pressure coefficient shown in figure 2 are representative. Only the curve for exact theory is affected by the value of M_1 and in the range $12 \lessapprox M_1 \leqq \infty$ the change in pressure coefficient with M_1 is very small (of the order of 0.01 to 0.02 except near shock detachment). Although this change has only a minor effect on the error curves at large values of δ, its effect at small values of δ is significant, as would be expected. This effect is illustrated for air and helium in figure 5 as a function of the similarity parameter K where the percent error in pressure coefficient at $M_1 = 20$ is shown for equations (3) and (6). These results show that the use of these equations for pressure predictions in the range $1 \ll M_1 \ll \infty$ should be restricted to $K \gtrapprox 3$. This restriction includes the prediction of pressure ratio p_2/p_1 by means of these equations; the percent error in pressure ratio is in very close agreement with the percent error in pressure coefficient for $K \gtrapprox 3$ and does not differ from the percent error in pressure coefficient by more than 5 percent until $K \lessapprox 1$. At very small values of δ the large percentage errors shown in figure 5 have little practical significance in view of the very small values of pressure coefficient. (See fig. 2.)

For the lower range of Mach numbers that are generally considered to fall within the hypersonic speed regime, another effect of γ may become significant. In order to illustrate this, both equations (3) and (6) may be regarded as special forms of the exact expression

$$C_{p,2} = \frac{4 \sin^2\epsilon}{\gamma + 1} - \frac{4}{(\gamma + 1)M_1^2} \tag{7}$$

in which the second term on the right has been dropped. The value of $C_{p,2}$ is less affected by the loss of this term when γ is large.

The preceding examples show that the value of γ and the configuration shape may have an important effect upon the accuracy of hypersonic approximations and that it may be desirable to use one expression for certain configurations and values of γ and another expression for other configurations and values of γ. The interest here is in the higher values of γ, specifically $\gamma = 7/5$ and $5/3$, where, with the exception of equation (1), the differences between the accuracies of the hypersonic approximations appear smaller, and where most of the approximations give the best predictions. The exception offered by equation (6) is minor since the error in its prediction for the largest value of γ is small until shock detachment is closely approached.

Differences between air and helium in changes across an oblique shock.- Preliminary insight into some aspects of air-helium differences and of the air-helium simulation problem may be gained by examining the changes that occur across an oblique shock as a function of the similarity parameter. From equation (2) the pressure ratio across an oblique shock at hypersonic speeds is given satisfactorily by

$$\frac{p_2}{p_1} = 1 + \gamma K^2 \left[\frac{\gamma + 1}{4} + \sqrt{\left(\frac{\gamma + 1}{4}\right)^2 + \frac{1}{K^2}} \right] \tag{8}$$

Other changes across an oblique shock may be obtained by the following exact expressions:

$$\frac{\rho_2}{\rho_1} = \frac{(\gamma + 1)\frac{p_2}{p_1} + (\gamma - 1)}{(\gamma - 1)\frac{p_2}{p_1} + (\gamma + 1)} \tag{9}$$

$$\frac{T_2}{T_1} = \frac{p_2}{p_1}\frac{\rho_1}{\rho_2} \tag{10}$$

$$\left(\frac{V_2}{V_1}\right)^2 = 1 - \frac{2\delta^2\left[\left(\frac{p_2}{p_1}\right)^2 - 1\right]}{K^2\left[(\gamma + 1)\frac{p_2}{p_1} + (\gamma - 1)\right]} \tag{11}$$

$$\frac{M_2}{M_1} = \frac{V_2}{V_1}\left(\frac{T_2}{T_1}\right)^{-1/2} \tag{12}$$

The results given by equations (8) to (12), with the aid of equation (2), are shown in figures 6 and 7 for air and helium for values of K from 0.1 to 10. Only the curves for $\delta = 0.2$ and $\delta = 0.4$ have been illustrated in figure 7; the left-hand limit of these curves is determined by the Mach number for shock detachment for these values of δ.

For $K \gtrapprox 3$ the following approximations are useful:

$$\frac{p_2}{p_1} = \frac{\gamma(\gamma + 1)K^2}{2} \tag{13}$$

$$\frac{\rho_2}{\rho_1} = \frac{1}{\frac{\gamma - 1}{\gamma + 1} + \frac{2}{\gamma(\gamma + 1)K^2}} \tag{14}$$

$$\frac{T_2}{T_1} = \frac{\gamma(\gamma - 1)K^2}{2} + 1 \tag{15}$$

$$\frac{V_2}{V_1} = \sqrt{1 - \gamma\delta^2} \tag{16}$$

$$\frac{M_2}{M_1} = \sqrt{\frac{2(1 - \gamma\delta^2)}{\gamma(\gamma - 1)K^2 + 2}} \tag{17}$$

For the same value of K in helium and in air[3] (i.e., $K_H = K_A$) the ratio of the pressure rise across the shock in helium to that in air is, therefore (for $K \gtrsim 3$),

$$\frac{\left(\frac{p_2}{p_1}\right)_H}{\left(\frac{p_2}{p_1}\right)_A} = \frac{\gamma_H(\gamma_H + 1)}{\gamma_A(\gamma_A + 1)} = 1.32 \tag{18}$$

For $K \gg 1$ and $K_H = K_A$, the following ratios are obtained. The density-rise ratio is

$$\frac{\left(\frac{\rho_2}{\rho_1}\right)_H}{\left(\frac{\rho_2}{\rho_1}\right)_A} = \left(\frac{\gamma + 1}{\gamma - 1}\right)_H \left(\frac{\gamma - 1}{\gamma + 1}\right)_A = 0.67 \tag{19}$$

The temperature-rise ratio is

$$\frac{\left(\frac{T_2}{T_1}\right)_H}{\left(\frac{T_2}{T_1}\right)_A} = \frac{\gamma_H(\gamma_H - 1)}{\gamma_A(\gamma_A - 1)} = 1.98 \tag{20}$$

The velocity-drop ratio is (for small to moderate values of δ)

$$\frac{\left(\frac{V_2}{V_1}\right)_H}{\left(\frac{V_2}{V_1}\right)_A} = 1 \quad \text{(for any two values of } \gamma\text{)} \tag{21}$$

The Mach number drop ratio is (for small to moderate values of δ)

---

[3]The subscripts H and A will be used to denote helium and air specifically, but note that the general expressions that are given in terms of γ are applicable to any two ideal gases having different values of γ.

$$\frac{\left(\frac{M_2}{M_1}\right)_H}{\left(\frac{M_2}{M_1}\right)_A} = \sqrt{\frac{\gamma_A(\gamma_A - 1)}{\gamma_H(\gamma_H - 1)}} = 0.71 \qquad (22)$$

The foregoing results show that most of the changes across an oblique shock at hypersonic speeds are significantly different in helium from those in air. Equations (8) to (17), and curves such as those shown in figures 6 and 7, may be used to establish the conditions for the air-helium simulation of the change in a given property across an oblique shock by determining the required ratio of K_H to K_A. In the following section the simulation conditions associated with the pressure rise across an oblique shock will be examined in detail. The simulation conditions for other changes across the shock may be derived in a similar manner.

L 4 1 6

Simulation of pressures and normal-force coefficients on a flat plate with zero sweep.- In the derivation of the simulation conditions, the use of the same hypersonic approximation for the two values of γ involved is, of course, preferable if the values of γ are such that the accuracy of the derived simulation conditions is not significantly affected. In the previous discussions of the γ effects upon the accuracy of the hypersonic approximations, equation (3) was noted to give, in general, slightly better predictions of pressure coefficient than equation (6) for $\gamma = 5/3$ (helium), the converse being true for $\gamma = 7/5$ (air). However, for either of these values of γ, the error in pressure coefficient introduced by the use of either equation for $K \gtrapprox 3$ remains below 10 percent until the flow deflection angles become of the order of those for shock detachment. In addition, neither equation appears to offer a significant advantage over the other in the accuracy of the simulation expressions that are derived; the simulation conditions are developed as a ratio of the value of a parameter in helium to its value in air, and, as will be illustrated subsequently, the value of this ratio is less sensitive to the choice of equations than are the values that form this ratio. Thus, the use of the same equation for helium and air appears permissible. In the derivations that follow equation (3) has been used because it yields simpler simulation expressions. The changes in these expressions that would result from the use of equation (6) instead of equation (3) may be readily evaluated since they would usually amount to no more than replacing δ by $\sin \delta$.

At hypersonic speeds the normal-force coefficient on a flat plate is for all practical purposes determined by the pressure on the high-pressure side of the plate. Thus, if the normal-force coefficient C_N

in a gas with a certain value of γ is to equal that in a gas with a different value of γ, then a sufficient condition is that the pressure coefficient C_p on the high-pressure side of the plate must be the same in the two gases. Thus, for $C_{N,H} = C_{N,A}$ it follows from equation (3) that the condition for simulation is

$$\frac{\delta_H}{\delta_A} = \sqrt{\frac{\gamma_A + 1}{\gamma_H + 1}} \tag{23}$$

Thus, for the same normal-force coefficient C_N in air and helium the angle of attack in helium should be 0.949 times that in air,[4] and this factor is independent of K for the conditions of this analysis ($K \gg 1$). It should be noted that, while equation (3) introduces large percentage errors in $C_{p,2}$ for $K \lesssim 3$, the percentage error in δ_H/δ_A that is incurred by use of equation (23) for $K \lesssim 3$ is small. In order to illustrate this, values of δ_H/δ_A have been computed by means of equation (2) and are given in the following table:

K	δ_H/δ_A
0	1
.1	.997
.5	.984
1	.972
3	.954
10	.949

It is apparent that equation (23), and other simulation expressions that will be derived from equation (3), may be used for values of K considerably less than 3 without introducing large error. Of equal importance is the implication that for $K \ll 1$ air and helium give essentially the same value of C_N; this is compatible with the result of linear theory that $C_{p,2}$ is independent of γ, as will be illustrated subsequently in the section entitled "Lift-drag ratio." The prediction of equation (23) is in good agreement with the value of 0.952 determined in reference 4

---

[4]If equation (6) had been used in this development, the factor 0.949 would equal $\frac{\sin \delta_H}{\sin \delta_A}$. However, the ratio δ_H/δ_A would obviously be little different. For example, with $\delta_A = 30^\circ$, the value of δ_H/δ_A would be 0.943 or less than 1 percent different from the value obtained by use of equation (3).

at Mach numbers of 12, 16, and 20 by shock-expansion calculations. Note that equation (23) does not make $\left(\frac{p_2}{p_1}\right)_H = \left(\frac{p_2}{p_1}\right)_A$.

If it is desired to have only $\left(\frac{p_2}{p_1}\right)_H = \left(\frac{p_2}{p_1}\right)_A$, then both M_1 and δ become variables in the simulation problem. From equation (13) the condition for simulation is

$$\frac{\delta_H}{\delta_A} = \frac{M_{1,A}}{M_{1,H}}\sqrt{\frac{\gamma_A(\gamma_A + 1)}{\gamma_H(\gamma_H + 1)}} \tag{24}$$

For air and helium,

$$\frac{\delta_H}{\delta_A} = 0.87\,\frac{M_{1,A}}{M_{1,H}} \tag{25}$$

thus offering a number of reasonable combinations. If $M_{1,H} = M_{1,A}$, then the angle of attack in helium should be 0.87 times that in air for simulation of $\frac{p_2}{p_1}$ only. (Note that $K_H/K_A = 0.87$.)

If it is desired to have $\left(\frac{p_2}{p_1}\right)_H = \left(\frac{p_2}{p_1}\right)_A$ and $C_{N,H} = C_{N,A}$ simultaneously, then two conditions must be satisfied. One is given by equation (23). The other condition is (substituting eq. (23) in eq. (24))

$$\frac{M_{1,H}}{M_{1,A}} = \sqrt{\frac{\gamma_A}{\gamma_H}} \tag{26}$$

For air and helium then, the angle of attack in helium should be about 0.95 times that in air, and the Mach number in helium should be about 0.92 times that in air for simulation of p_2/p_1 and C_N simultaneously.

Another condition of simulation which may be of interest is to have $C_{N,H} = C_{N,A}$ and $\delta_H = \delta_A$. An examination shows that the values of $\frac{M_{1,H}}{M_{1,A}}$ necessary for this simulation cannot be evaluated accurately by the use of hypersonic approximations, although trends may be established which

show that $\frac{M_{1,H}}{M_{1,A}}$ becomes increasingly large as $\delta M_{1,A}$ increases.[5] This inaccuracy should not be interpreted as a significant deficiency of hypersonic approximations, since it is caused by the very small effect that large changes in M_1 have upon C_N at a given value of δ when $M_1 \gg 1$. Accordingly, small errors in C_N may show up as large errors in $\frac{M_{1,H}}{M_{1,A}}$. To this end, it may be shown from equation (3) that, for $\delta_H = \delta_A$,

$$\frac{C_{N,H}}{C_{N,A}} = \frac{\gamma_H + 1}{\gamma_A + 1} \tag{27}$$

which shows that, provided $K \gg 1$, $C_{N,H}$ will at most be only about 11 percent greater than $C_{N,A}$ when simulation is disregarded altogether.[6] Thus, this form of simulation is not so unattractive as the values of $\frac{M_{1,H}}{M_{1,A}}$ for simulation might first imply, in that by a selection of a reasonable value of $\frac{M_{1,H}}{M_{1,A}}$ (although this value may be far from the exact value) $C_{N,H}$ may differ from $C_{N,A}$ by only 1 percent or so.

Simulation of normal-force coefficients on thick flat plates.- In reference 4 a study was made by shock-expansion theory to determine the values of the ratio of angle of attack in helium to that in air necessary to give $C_{N,H} = C_{N,A}$ for two-dimensional 10-percent-thick plates with wedge and parabolic leading edges. The leading-edge half-angle θ was

---

[5]Exact calculations for a flat plate at 6° angle of attack show that $\frac{M_{1,H}}{M_{1,A}}$ is about 1 at $M_{1,A} = 10$, 1.1 at $M_{1,A} = 16$, and about 1.4 at $M_{1,A} = 25$. At $\alpha = 12°$, $\frac{M_{1,H}}{M_{1,A}}$ is about 1.7 at $M_{1,A} = 12$.

[6]For $M_{1,H} = M_{1,A}$ and conditions compatible with equation (27), the shock angle is given by $\epsilon = \frac{\gamma + 1}{2}\delta$. Thus, $\epsilon_H/\epsilon_A = \frac{\gamma_H + 1}{\gamma_A + 1}\frac{\delta_H}{\delta_A}$ which for $\delta_H = \delta_A$ gives the same result as equation (27) (i.e., $\epsilon_H \epsilon_A = C_{N,H}/C_{N,A} = 1.11$). Note, however, that the simulation of shock angles requires that $\frac{\delta_H}{\delta_A} = \frac{\gamma_A + 1}{\gamma_H + 1}$ and that this is the square of the δ ratio for simulation of C_N. (See eq. (23).)

varied from 0° to 30° for the wedge-nose plates; for the parabolic-nose plates, leading-edge half-angles of about 11° and 24° were examined for comparison with the results for the wedge leading edge. The calculations covered Mach numbers of 12, 16, and 20. The ratio α_H/α_A determined by these calculations is shown in figure 8. All the results fall essentially on a single curve; it would therefore appear reasonable to regard this curve as applicable for Mach numbers of the order of 10 and greater. It is interesting to note that within the restrictions of this study, nose shape (parabolic or wedge) has no effect on α_H/α_A when the angle at the leading edge is the same.

With respect to the decrease in α_H/α_A with increasing θ shown for these thick plates, tangent-wedge theory indicates that for slender wedges with $\alpha < \theta$ the ratio α_H/α_A is independent of θ and is equal to $\frac{\gamma_H + 1}{\gamma_A + 1}$, or 0.90 (for $\theta_H = \theta_A$). However, for slender wedges with $\alpha > \theta$, the effect of θ is qualitatively the same as that shown in figure 8; tangent-wedge theory yields (for $\theta_H = \theta_A$)

$$\frac{\alpha_H}{\alpha_A} = \left(\frac{\gamma_A + 1}{\gamma_H + 1}\right)^{1/2}\left(1 + \frac{\theta}{\alpha_A}\right) - \frac{\theta}{\alpha_A} \tag{28}$$

or

$$\frac{\alpha_H}{\alpha_A} = 0.949 - 0.051\,\frac{\theta}{\alpha_A} \tag{29}$$

Thus, within the applicable limits of $\frac{\theta}{\alpha_A}$ $\left(\text{i.e., } 0 \leq \frac{\theta}{\alpha_A} \leq 1\right)$ increasing θ at constant α reduces α_H/α_A from its flat-plate value. For example, with $\alpha_A = 8.5°$ and therefore $\theta \leq 8.5°$ the variation of α_H/α_A with θ given by equation (29) is about the same as that shown in figure 8.

Simulation for flat plates or wedges with sweep.- In reference 22, expressions have been developed for obtaining the pressure associated with sweptback, attached, oblique shocks and flow deflections at hypersonic speeds. These expressions may be used to obtain simulation conditions for different values of γ. Only the case of $M_1 \to \infty$ is considered herein.

From reference 22,

$$\frac{C_{p,2}}{\delta^2} = \frac{2}{1 + \psi^2}\left[1 + \frac{1 - \sqrt{1 - (\gamma^2 - 1)\psi^2}}{(\gamma + 1)\psi^2}\right] \tag{30}$$

where ψ is the flow-deflection—sweep parameter and is equal to $\delta \tan \Lambda$ (Λ is the angle of sweepback).

For zero sweep ($\psi = 0$), equation (30) reduces to equation (3). For maximum sweep (i.e., detachment) $\psi_{max} = (\gamma^2 - 1)^{-1/2}$, and the pressure coefficient for ψ_{max} is (ref. 22)

$$C_{p,2} = 2\delta^2\left(\gamma - \frac{1}{\gamma}\right) \tag{31}$$

In figure 9 curves calculated from equation (30) for helium and air are presented. These curves may be used to obtain simulation of $C_{p,2}$ and, therefore, of C_N for swept flat plates at angle of attack or for swept wedges when the low-pressure side of the wedge is at zero angle of attack or operates in the "hypersonic shadow." For example, the ratio δ_H/δ_A for $(C_{p,2})_H = (C_{p,2})_A$ and $\psi_H = \psi_A$ may be obtained from the curves; this ratio is also given by the relation

$$\left(\frac{\delta_H}{\delta_A}\right)^2 = \frac{\gamma_H + 1}{\gamma_A + 1}\left[\frac{(\gamma_A + 1)\psi^2 + 1 - \sqrt{1 - (\gamma_A^2 - 1)\psi^2}}{(\gamma_H + 1)\psi^2 + 1 - \sqrt{1 - (\gamma_H^2 - 1)\psi^2}}\right] \tag{32}$$

which for zero sweep reduces to equation (23). Note that when simulation is achieved with $\psi_H = \psi_A$, the relation between sweep and angle of attack is

$$\frac{\delta_H}{\delta_A} = \frac{\tan \Lambda_A}{\tan \Lambda_H} \tag{33}$$

Consequently, for the simulation with $\psi_H = \psi_A$, neither the angle of attack nor the sweep angle can be the same in helium as in air. Figure 10 gives the ratio δ_H/δ_A for this simulation; there is no large variation in the value of δ_H/δ_A for simulation until detachment is approached. It should be noted, however, that within detachment limits it is impossible to obtain values of ψ in helium as high as those that can be

obtained in air. (See fig. 9.) Equation (4) may be used to show that the value of δ_H for detachment is about 0.81 times the value of δ_A for detachment.

The condition of having neither δ nor Λ the same in air and helium may not be desirable in some studies. It may be preferable to have $\Lambda_H = \Lambda_A$ or $\delta_H = \delta_A$, in which cases $\psi_H \neq \psi_A$. Consider first the case of equal sweep angles $\Lambda_H = \Lambda_A$. Observe that when $\psi_H \neq \psi_A$ and $\Lambda_H = \Lambda_A$, the following equation results:

$$\frac{\psi_H}{\psi_A} = \frac{\delta_H}{\delta_A} \tag{34}$$

The condition that $\left(C_{p,2}\right)_H = \left(C_{p,2}\right)_A$ may be written as

$$\delta_H{}^2\left[\frac{\left(C_{p,2}\right)_H}{\delta_H{}^2}\right] = \delta_A{}^2\left[\frac{\left(C_{p,2}\right)_A}{\delta_A{}^2}\right] \tag{35}$$

from which it follows, with equation (34), that

$$\frac{\psi_H{}^2}{\psi_A{}^2} = \frac{\left(C_{p,2}\right)_A/\delta_A{}^2}{\left(C_{p,2}\right)_H/\delta_H{}^2} \tag{36}$$

This expression for simulation is chosen since it facilitates the use of the results obtained from equation (30) and shown in figure 9. For demonstration, consider that the angle of attack in air and the sweep angle are known. Thus, $\psi_A = \delta_A \tan \Lambda_A$ is known, as is $\left(C_{p,2}\right)_A$. It is desired to know δ_H/δ_A for the simulation of $C_{p,2}$. Since the value of the parameter $\psi_A{}^2\left[\frac{\left(C_{p,2}\right)_A}{\delta_A{}^2}\right]$ is known, it is sufficient to determine the value of ψ_H that will give the same value of this parameter in helium. By use of equations (30) and (36) an expression relating ψ_H to the known quantities can be obtained; however, the expression is cumbersome to use. A more convenient method is to use the results given in figure 9 to plot curves of $\psi^2 \frac{C_{p,2}}{\delta^2}$ as a function of ψ. This has been done in figure 11. From these curves the angle-of-attack ratio (see eq. (34)) can be obtained by noting the values of ψ that correspond

to a given value of $\psi^2 \frac{C_{p,2}}{\delta^2}$. For helium and air the ratio $\frac{\psi_H}{\psi_A} = \frac{\delta_H}{\delta_A}$ is given in figure 12 as a function of $\psi^2 \frac{C_{p,2}}{\delta^2}$. Again, the variation in δ_H/δ_A is not large until detachment is approached; therefore, an average value of δ_H/δ_A taken over a given range of interest for $\psi^2 \frac{C_{p,2}}{\delta^2}$, which equals $C_{p,2} \tan^2\Lambda$, would give reasonable simulation, provided that the range is not too large. Also, as before, it is impossible within detachment limits to obtain values of ψ or $\psi^2 \frac{C_{p,2}}{\delta^2}$ with helium as high as those than can be reached in air. (See fig. 11.)

For the case of $\psi_H \neq \psi_A$ and $\delta_H = \delta_A$ the ratio of the sweep angles Λ_H/Λ_A may be obtained by noting that in this case

$$\frac{\psi_H}{\psi_A} = \frac{\tan \Lambda_H}{\tan \Lambda_A} \tag{37}$$

With this relation the curves of figure 9 may be used to show that $\frac{\tan \Lambda_H}{\tan \Lambda_A}$ is always greater than unity; that is, the sweep angle must be larger in helium than in air for this method of simulation. The curves of figure 9 also show that this method of simulation is more restricted than the other methods in the range of ψ and C_p/δ^2 that it is able to cover.

Although certain areas of restriction have been pointed out in the above simulations, it is well to bear in mind that partial simulations in the direction indicated may often yield adequate results, since with no simulation (i.e., $\delta_H = \delta_A$, $\Lambda_H = \Lambda_A$, and, therefore, $\psi_H = \psi_A$) the value of $\frac{C_{p,2}}{\delta^2}$ for helium ranges only from about 11 percent greater than that for air at $\psi = 0$ to about 15 percent greater at $\psi = 0.6$.

Drag coefficients for cones and wedges at zero angle of attack.- Several approximations exist for the drag coefficients of cones and wedges at hypersonic speeds (e.g., see refs. 19, 23, 24, and 25). These approximations may be used to obtain the ratio of the drag coefficient in helium to that in air. The expressions given in reference 19 have been selected for this purpose since they give results that are either the same as or slightly better than the results given by the other sources.

The ratio of the drag coefficients for cones may be shown to be, for $\theta_H = \theta_A$,

$$\frac{C_{D,H}}{C_{D,A}} = \left[\frac{(\gamma + 1)(\gamma + 7)}{(\gamma + 3)^2}\right]_H \left[\frac{(\gamma + 3)^2}{(\gamma + 1)(\gamma + 7)}\right]_A = 1.02 \qquad (38)$$

For wedges, with $\theta_H = \theta_A$,

$$\frac{C_{D,H}}{C_{D,A}} = \frac{\gamma_H + 1}{\gamma_A + 1} = 1.11 \qquad (39)$$

In figure 13 a comparison of these approximations with exact solutions is presented. The fact that the exact solutions are for $M_1 = 20$ rather than $M_1 = \infty$ does not significantly affect the assessment of the approximations. The approximation of $\frac{C_{D,H}}{C_{D,A}}$ for cones is seen to be generally better than that for wedges. From these results the drag coefficients for cones may be concluded to be about 2 percent greater in helium than those in air and the drag coefficients for wedges to be some 11 percent greater in helium than those in air, unless the nose angle comes within a few degrees of that producing shock detachment in helium, or is very small.

The ratios shown in figure 13 may be used as correction factors in interpreting helium results in terms of air results. The ratio for cones is, except at large values of θ, so near unity that it could probably be neglected in many studies.

Since cone or wedge drag coefficients can be simulated in helium by changes in the value of θ, an evaluation has been made of the magnitude of the change required for $C_{D,H} = C_{D,A}$. Exact calculations at $M_1 = 20$ give the following results for $C_{D,H} = C_{D,A}$:

θ_A, deg	$(\theta_H/\theta_A)_{cones}$	$(\theta_H/\theta_A)_{wedges}$
20	0.988	0.945
28	.987	.934
34	.984	.919

The ratio θ_H/θ_A is seen to be relatively insensitive to the value of θ_A. Note that for the highest value of θ_A considered, θ_H is less than θ_A by only about 0.5° for cones and by about 2.7° for wedges.

The ratio of θ_H/θ_A for $C_{D,H} = C_{D,A}$ may also be obtained by use of the approximations that yield equations (38) and (39). The value of this ratio is about 0.99 for cones and 0.95 for wedges. These values compare favorably with the exact values in the preceding table except for wedges with large values of θ.

L
4
1
4

Simulation for blunt bodies.-

Preliminary remarks: The discussions thus far have dealt with conditions associated with attached shocks and, therefore, with a configuration with a sharp leading edge or pointed nose. Some of the air-helium differences and simulation problems common to blunt bodies with detached shocks will now be examined. One of the differences between air and helium that is immediately apparent is the difference in the maximum density rise across a normal shock $\left(\text{i.e., } \frac{\rho_2}{\rho_1} = 6 \text{ for air and } 4 \text{ for helium}\right)$. Although this difference might be expected to cause significant differences for $M_1 \gg 1$ in such features as shock detachment distance, flow fields, shock shape, and the like, it should not be interpreted as implying that no simulation is possible in helium for Mach numbers in air that give $\frac{\rho_2}{\rho_1} > 4$ or that the differences between air and helium results are necessarily large. Adequate simulation of some of these features can be achieved, particularly in local regions; when simulation cannot be achieved, adequate transformation of the helium results to air results is often possible.

Pressures across shock layer at axis of symmetry: Consider the blunt nose at hypersonic speeds with detached shock as shown in the following sketch:

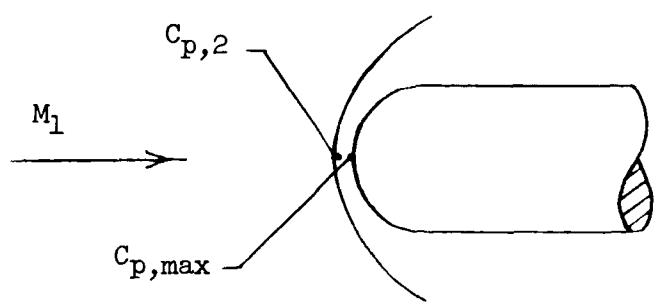

According to Newtonian theory[7] the pressure coefficient at the stagnation point $C_{p,max}$ has a value of 2. However, better results are obtained by use of the value of $C_{p,max}$ suggested in the blunt-nose modification of Newtonian theory of reference 19, which for $M_1 \gg 1$ reduces to $\frac{\gamma + 3}{\gamma + 1}$, thus yielding as the blunt-nose modified Newtonian theory

$$C_p = \frac{\gamma + 3}{\gamma + 1} \sin^2\delta \tag{40}$$

The value of $C_{p,max}$ in this expression is satisfactory for helium as well as for air even at moderate hypersonic speeds.[8]

Thus,

$$\frac{(C_{p,max})_H}{(C_{p,max})_A} = \left(\frac{\gamma + 3}{\gamma + 1}\right)_H \left(\frac{\gamma + 1}{\gamma + 3}\right)_A = 0.954 \tag{41}$$

The pressure coefficient immediately behind the normal shock for $M_1 \gg 1$ may be shown from the exact shock equations to reduce to

$$C_{p,2} = \frac{4}{\gamma + 1} \tag{42}$$

---

[7]In application to blunt and pointed bodies equation (1) may be expressed in the more versatile form $C_p = C_{p,max} \frac{\sin^2\delta}{\sin^2\delta_{max}}$. For pointed bodies δ_{max} is the surface angle at the nose, and $C_{p,max}$ is the pressure coefficient on the surface at this point (exact value of $C_{p,max}$ should be used). For blunt bodies ($\delta_{max} = 90^\circ$) this expression reduces to equation (1) when the value of $C_{p,max}$ is the Newtonian value.

[8]For example, at $M_1 = 8$ the exact value of $C_{p,max}$ is 1.752 for helium and 1.826 for air. Equation (40) gives 1.750 for helium and 1.833 for air. When $M_1 \to \infty$, the values of $C_{p,max}$ given by $C_{p,max} = 2\left[\left(\frac{\gamma + 1}{2}\right)^{\frac{\gamma+1}{\gamma-1}} (\gamma)^{-\frac{\gamma}{\gamma-1}}\right]$ are slightly more accurate than those used in equation (40). The exact ratio of $C_{p,max}$ in helium to that in air, at $M_1 = 8$, is 0.959 (compare this value with eq. (41)).

Thus,

$$\frac{(C_{p,2})_H}{(C_{p,2})_A} = \frac{\gamma_A + 1}{\gamma_H + 1} = 0.90 \tag{43}$$

From these results, the values of C_p through the shock layer along the axis of symmetry vary from values that are about 10 percent less in helium than in air just behind the shock to values that are about 5 percent less in helium than in air at the stagnation point. Thus, hypersonic studies in helium in this vicinity of a blunt nose will not be subject to large differences in the values of the pressure coefficients from those obtained in air. Corrections to helium results of the magnitude just indicated may be used to minimize these differences.

Shock detachment distance: The shock detachment distance d on the axis of symmetry may be calculated by a number of methods. Although the value of d appears to vary somewhat with the method used, the ratio of d_H/d_A appears relatively independent of the method. (For example, compare refs. 26 and 27.) The method of reference 27 will be used herein for the nearly circular or spherical nose. For the two-dimensional case this method gives

$$\frac{d}{r_s} = \frac{k}{1 - k} \sinh^{-1}\left[\frac{1 - k}{\sqrt{k(2 - k)}}\right] \tag{44}$$

where r_s is the radius of curvature of the shock at the axis (taken to be the same as that of the body for computations) and k is the inverse of the density rise across the shock at the axis (i.e., $k = \rho_1/\rho_2$). For $M_1 \gg 1$, $k = \frac{\gamma - 1}{\gamma + 1}$. The negative sign convention for r_s employed in reference 27 is not used herein. From equation (44) there is thus obtained for the nearly circular two-dimensional nose

$$\frac{\left(\frac{d}{r_s}\right)_H}{\left(\frac{d}{r_s}\right)_A} = 1.35 \tag{45}$$

The detachment distance for the nearly spherical axisymmetric nose is

$$\frac{d}{r_s} = k\left[\frac{1 - \sqrt{1 - (1 - k)^2}}{(1 - k)^2}\right] \tag{46}$$

from which there is obtained

$$\frac{\left(\frac{d}{r_s}\right)_H}{\left(\frac{d}{r_s}\right)_A} = 1.40 \tag{47}$$

For flat-nosed two-dimensional bodies the detachment distance is given by (ref. 28; this reference was unpublished at the time this paper was prepared, but galley proofs were available to the authors through the courtesy of Dr. R. W. Truitt)

$$\frac{d}{a} = \left(\frac{2}{\gamma + 1}\right)^{-\frac{1}{\gamma-1}\sqrt{k}} \tag{48}$$

where a is the half height of the body. This expression yields for $M_1 \gg 1$

$$\frac{\left(\frac{d}{a}\right)_H}{\left(\frac{d}{a}\right)_A} = 1.19 \tag{49}$$

This ratio may be observed to be equal to the ratio of the values of γ for helium and air, but this appears to be a coincidence in that other combinations of γ that have been examined do not give this result.

For nearly flat-nosed axisymmetric bodies, reference 29 gives

$$\frac{d}{a} = 1.03\sqrt{\frac{\gamma - 1}{2}} \tag{50}$$

from which it follows that

$$\frac{\left(\frac{d}{a}\right)_H}{\left(\frac{d}{a}\right)_A} = \sqrt{\frac{\gamma_H - 1}{\gamma_A - 1}} = 1.29 \tag{51}$$

These results show that the shock is always further removed from the nose of a given body in helium than in air and that the difference between the detachment distances in air and helium is greater when the body is axisymmetric. It is thus evident that the duplication of detachment distance in helium and air would require that the model in helium have either a smaller radius of curvatuve, or smaller half height, than the model in air. For most studies, however, the primary interest is

directed toward simulation of conditions on the body surface. If these conditions can be simulated, or if there is little difference between air and helium without simulation, lack of simulation of detachment distance appears relatively unimportant. Some aspects of conditions at the body surface will be considered next.

Pressure and Mach number distribution: If the pressure distribution over rounded blunt noses obeys the blunt-nose modified Newtonian theory, that is,

$$\frac{C_p}{C_{p,max}} = \cos^2\varphi \tag{52}$$

where φ is the angle between free-stream direction and the normal to the body surface, then the transformation of the pressure distribution from one value of γ to another is readily accomplished by use of equation (40). Note that so long as the ratio $C_p/C_{p,max}$ can be expressed as any function of body shape only, this transformation would probably apply.

For $C_{p,H} = C_{p,A}$ equation (52) shows that

$$\frac{\cos \varphi_H}{\cos \varphi_A} = 1.023 \tag{53}$$

The following table gives values of φ_H/φ_A for $C_{p,H} = C_{p,A}$ as a function of φ_A. The minimum value of $\varphi_A = 12.3^\circ$ is that for which $(C_{p,max})_H = C_{p,A}$. Values of φ_A beyond 50° have not been considered since equation (52) is generally inadequate beyond about 55°.

φ_A, deg	φ_H/φ_A
12.3	0
15	.592
20	.800
30	.922
40	.959
50	.978

These results reflect the effect of the lower value of $C_{p,max}$ in helium, in that a given value of C_p occurs at a position that is nearer the stagnation point in helium than it is in air. Also, the difference

between φ_H and φ_A for $C_{p,H} = C_{p,A}$ decreases with increasing φ. Note, however, that for $\varphi_H = \varphi_A$,

$$\frac{C_{p,H}}{C_{p,A}} = \frac{\left(C_{p,max}\right)_H}{\left(C_{p,max}\right)_A} \tag{54}$$

Consequently, for a given value of φ, $C_{p,H}$ is only about 5 percent less than $C_{p,A}$. (See eq. (42).)

The Mach number distribution may be obtained from equation (52) by noting that for $M_1 \gg 1$

$$\cos^2\varphi = \frac{p}{p_{max}} \tag{55}$$

It follows that

$$\cos^2\varphi = \left(1 + \frac{\gamma - 1}{2} M^2\right)^{-\frac{\gamma}{\gamma-1}} \tag{56}$$

and

$$M^2 = \frac{2}{\gamma - 1}\left[\frac{1}{(\cos^2\varphi)^{\frac{\gamma-1}{\gamma}}} - 1\right] \tag{57}$$

For M_H to equal M_A, the relation between φ_H and φ_A is thus

$$\cos\varphi_H = \left\{1 + \frac{\gamma_H - 1}{\gamma_A - 1}\left[\frac{1}{\left(\cos^2\varphi_A\right)^{\frac{\gamma_A-1}{\gamma_A}}} - 1\right]\right\}^{-\frac{\gamma_H}{2(\gamma_H-1)}} \tag{58}$$

The following table gives values of φ_H/φ_A for $M_H = M_A$ as a function of φ_A:

φ_A, deg	φ_H/φ_A
5	1.090
10	1.089
20	1.084
30	1.073
40	1.060
50	1.044

As φ_A approaches 0°, $\frac{\varphi_H}{\varphi_A} = \left(\frac{\gamma_H}{\gamma_A}\right)^{1/2} = 1.091$. The value of φ_H/φ_A is seen to experience a small decrease as φ_A increases and may be considered essentially constant over a large portion of the nose.

For $\varphi_H = \varphi_A$ the value of M_H/M_A is given by

$$\left(\frac{M_H}{M_A}\right)^2 = \left(\frac{\gamma_A - 1}{\gamma_H - 1}\right)\left[\frac{1 - \left(\cos^2\varphi\right)^{\frac{\gamma_H - 1}{\gamma_H}}}{1 - \left(\cos^2\varphi\right)^{\frac{\gamma_A - 1}{\gamma_A}}}\right]\left(\cos^2\varphi\right)^{\frac{\gamma_A - \gamma_H}{\gamma_A \gamma_H}} \tag{59}$$

The following table gives values of M_H/M_A for $\varphi_H = \varphi_A$ as a function of φ:

φ, deg	M_H/M_A
5	0.917
10	.918
20	.919
30	.924
40	.931
50	.940

As φ approaches 0°, $\frac{M_H}{M_A} = \left(\frac{\gamma_A}{\gamma_H}\right)^{1/2} = 0.917$. The value of M_H/M_A is seen to experience a small increase as φ increases and may be considered essentially constant over a large portion of the nose. Both of the preceding tables indicate that the differences in Mach number distribution between air and helium are small and that a given value of

Mach number occurs at a position that is slightly farther away from the stagnation point in helium than it is in air (the reverse of the behavior of C_p). In this regard, equation (56) places the sonic point on the body[9] at (the same result is obtained in refs. 27 and 30)

$$\cos \varphi' = \left(\frac{2}{\gamma + 1}\right)^{\frac{\gamma}{2(\gamma-1)}} \tag{60}$$

which yields $\varphi_H' = 45.8^\circ$ and $\varphi_A' = 43.4^\circ$, or $\varphi_H'/\varphi_A' = 1.055$.

The results of studies of flat noses indicate, as might be expected, that the surface pressure distribution in the vicinity of the stagnation point is a function only of position and $C_{p,max}$. (For example, see ref. 31.) Therefore, for a given position on the flat nose near the stagnation point, the ratio of $C_{p,H}$ to $C_{p,A}$ is expressed by equation (54).

Velocity gradient: The value of the velocity gradient is important in skin-friction and heat-transfer problems. In reference 32 the velocity gradient on a nearly circular blunt nose has been derived on the basis of blunt-nose modified Newtonian theory. This result is referenced to the pressure and density at the stagnation point, p_{max} and ρ_{max}, and for $M_1 \gg 1$ may be reduced to

$$\frac{du}{dx} = \frac{\sqrt{2}}{r}\sqrt{\frac{p_{max}}{\rho_{max}}}\left[\frac{\left(\frac{\gamma - 1}{\gamma}\right)\left(\frac{p}{p_{max}}\right)^{\frac{\gamma-2}{\gamma}}\left(1 - \frac{p}{p_{max}}\right)}{1 - \left(\frac{p}{p_{max}}\right)^{\frac{\gamma-1}{\gamma}}}\right]^{1/2} \tag{61}$$

where x is distance parallel to body surface and r is the radius of curvature of the nose surface. Substituting equation (55) into equation (61) and rearranging yields

---

[9]The sonic point on the shock ahead of a nearly spherical nose occurs, according to reference 30, at $\varphi \approx \sqrt{k}$. Thus, on the shock

$$\frac{\varphi_H'}{\varphi_A'} = \left[\left(\frac{\gamma - 1}{\gamma + 1}\right)_H\left(\frac{\gamma + 1}{\gamma - 1}\right)_A\right]^{1/2} = 1.23.$$

$$r\frac{du}{dx}\left(\frac{p_{max}}{\rho_{max}}\right)^{-1/2} = \left[\frac{2\left(\frac{\gamma-1}{\gamma}\right)\left(\cos^2\varphi\right)^{\frac{\gamma-2}{\gamma}}\left(1-\cos^2\varphi\right)}{1-\left(\cos^2\varphi\right)^{\frac{\gamma-1}{\gamma}}}\right]^{1/2} \qquad (62)$$

With U representing the left-hand side of this equation, the following table gives the ratio U_H/U_A as a function of φ, for $\varphi_H = \varphi_A$:

φ, deg	U_H/U_A
5	0.999
10	.997
20	.989
30	.975
40	.955
50	.926

At the stagnation point ($\varphi = 0^\circ$), the value of U is independent of γ and is equal to $\sqrt{2}$ (ref. 32). Thus, when the velocity-gradient parameter is expressed in the form of U, these results show that there is essentially no difference between air and helium over a large portion of the nose. At the sonic point on the nose

$$U' = \left\{2\left(\frac{\gamma+1}{\gamma}\right)\left[1-\left(\frac{2}{\gamma+1}\right)^{\frac{\gamma}{\gamma-1}}\right]\left(\frac{2}{\gamma+1}\right)^{\frac{\gamma-2}{\gamma-1}}\right\}^{1/2} \qquad (63)$$

from which $U_H' = 1.377$ and $U_A' = 1.458$, or $U_H'/U_A' = 0.944$. (Recall from eq. (60) that the location of the sonic point in helium is farther around the body than it is in air, but only by about 2.4° in φ.) These values illustrate, by comparison with the value of $\sqrt{2}$ at the stagnation point, an interesting result of equation (62), namely, that whereas for air the value of U increases as φ increases, for helium the value of U decreases as φ increases.[10] As shown, however, the differences in U between air and helium are still small at the sonic point.

---

[10]For γ near 1.54 there is little change in U with φ over the range of φ considered herein, $0^\circ \leqq \varphi \lessapprox 50^\circ$.

It is of interest to compare the preceding results with those given by another much-used form of the velocity-gradient parameter as given in reference 19 for a rounded nose. For this comparison only the stagnation point will be considered. This parameter will be denoted by $\tilde{U}$ to distinguish it from U, and for $M_1 \gg 1$ the value at the stagnation point for a two-dimensional or axisymmetric nose is given by

$$\tilde{U} \equiv \frac{D}{u_2}\frac{du}{dx} = \frac{2(\gamma + 1)}{\sqrt{\gamma(\gamma - 1)}} \tag{64}$$

where D is the diameter of the nose and u_2 is the axial velocity just behind the shock wave. The ratio $\tilde{U}_H/\tilde{U}_A$ is thus 0.789 and is not to be compared with the ratio $U_H/U_A = 1$ given by equation (62) for the stagnation point because of the difference in the reference quantities.

Both U and $\tilde{U}$ may be referenced to free-stream conditions as follows. First, consider $\tilde{U}$. Conservation of mass across the shock requires that $\rho_1 u_1 = \rho_2 u_2$. For $M_1 \gg 1$, $\rho_1/\rho_2 = k = u_2/u_1$. Thus,

$$\tilde{U}_1 \equiv \frac{D}{u_1}\frac{du}{dx} = \frac{D}{u_2}\frac{du}{dx}\,k = 2\sqrt{\frac{\gamma - 1}{\gamma}} \tag{65}$$

Therefore, with $\tilde{U}$ referenced to free-stream velocity,

$$\frac{\tilde{U}_{1,H}}{\tilde{U}_{1,A}} = \left(\frac{\gamma_H - 1}{\gamma_A - 1}\frac{\gamma_A}{\gamma_H}\right)^{1/2} = 1.183 \tag{66}$$

Next, consider U. With the aid of equation (40), the density ratio k, and the relation $u_1 = M_1\sqrt{\gamma\frac{p_1}{\rho_1}}$, there is obtained, for $M_{1,H} = M_{1,A}$,

$$\left[\frac{\left(\frac{p_{max}}{\rho_{max}}\right)_H}{\left(\frac{p_{max}}{\rho_{max}}\right)_A}\right]^{1/2} = \frac{u_{1,H}}{u_{1,A}}\left(\frac{\gamma_A + 1}{\gamma_H + 1}\right)\left[\frac{(\gamma_H + 3)(\gamma_H - 1)}{(\gamma_A + 3)(\gamma_A - 1)}\right]^{1/2} \tag{67}$$

L
4
1
4

Since at the stagnation point $\frac{U_H}{U_A} = 1$, equation (67) shows that, with U_l denoting reference to free-stream velocity, $\frac{U_{l,H}}{U_{l,A}} = 1.197$. This value agrees closely with the result of equation (66). Thus, the two expressions for the velocity gradient that have been considered give the same result within the accuracy of the approximations, at least at the stagnation point, if the same reference quantities are used. When referenced to free-stream conditions, the velocity-gradient parameter at the stagnation point is greater in helium than in air. However, the necessary change in D or u_l for simulation is easily obtained from the results that have been presented.

L
4
1
4

The preceding conclusions also apply to the stagnation point for a nearly flat nose, for which the results of reference 31 may be used to show that

$$\frac{\tilde{U}_{l,H}}{\tilde{U}_{l,A}} = \frac{\left[k(2 - k)\right]_H^{1/2}}{\left[k(2 - k)\right]_A^{1/2}} \tag{68}$$

or

$$\frac{\tilde{U}_{l,H}}{\tilde{U}_{l,A}} = \left\{\left[\frac{(\gamma - 1)(\gamma + 3)}{(\gamma + 1)^2}\right]_H \left[\frac{(\gamma + 1)^2}{(\gamma - 1)(\gamma + 3)}\right]_A\right\}^{1/2} = 1.197 \tag{69}$$

Thus, the value of $\tilde{U}_{l,H}/\tilde{U}_{l,A}$ at the stagnation point is, within the accuracy of the approximations, the same for rounded and flat noses. (Compare with eq. (66) and the value of $U_{l,H}/U_{l,A}$.)

Mass flow along surface: Another important quantity in studies of aerodynamic heating, coolant effectiveness, and the like is the inviscid mass flow $\rho_l u_l$ along the surface (at the outer edge of the boundary layer). From Newtonian theory, reference 33 gives the ratio of local mass flow just outside the boundary layer to the free-stream mass flow as

$$\tilde{m}_l \equiv \frac{\rho_l u_l}{\rho_l u_l} = \left(\cos^2\varphi\right)^{1/\gamma}\left[1 - \left(\cos^2\varphi\right)^{\frac{\gamma-1}{\gamma}}\right]^{1/2}\left(\frac{\gamma + 1}{2}\right)^{\frac{\gamma+1}{\gamma-1}}\left(\frac{2}{\gamma - 1}\right)\gamma^{-\frac{1}{\gamma-1}} \tag{70}$$

The following table gives values of mass-flow ratio $\tilde{m}_{l,H}/\tilde{m}_{l,A}$ as a function of φ:

φ, deg	$\tilde{m}_{l,H}/\tilde{m}_{l,A}$
5	0.811
10	.814
20	.820
30	.832
40	.848
50	.875

As φ approaches 0°, $\tilde{m}_{l,H}/\tilde{m}_{l,A} = 0.810$.

Since the maximum value of $\rho_l u_l$ occurs at the sonic point, the value of the mass-flow ratio at this point is of interest. Equation (70) yields $\tilde{m}'_{l,H}/\tilde{m}'_{l,A} = 0.860$. These results show that for the same free-stream mass flows, the local mass flows on the blunt nose are significantly less in helium than in air. In other words, $(\rho_l u_l)_H$ must be greater than $(\rho_l u_l)_A$ to achieve simulation of local mass flows on the nose; for simulation at the sonic point $(\rho_l u_l)_H/(\rho_l u_l)_A$ must equal about 1.16. With respect to simulation, the preceding table shows that $\tilde{m}_{l,H}/\tilde{m}_{l,A}$ experiences small changes with φ.

The local mass flow, like the velocity gradient, is often referenced to $p_{max}\rho_{max}$. In order to illustrate the differences that result when the local mass flow is referenced to $p_{max}\rho_{max}$ instead of $\rho_l u_l$, the sonic point will be used. Reference 32 gives

$$m' \equiv \frac{\rho_l' u_l'}{\sqrt{p_{max}\rho_{max}}} = \sqrt{\gamma}\left(\frac{2}{\gamma + 1}\right)^{\frac{\gamma+1}{2(\gamma-1)}} \tag{71}$$

from which $m_H'/m_A' = 1.061$. This result may be transformed, so that $\rho_l u_l$ is the reference quantity, by the relation

$$\left[\frac{(p_{max}\rho_{max})_H}{(p_{max}\rho_{max})_A}\right]^{1/2} = \frac{(\rho_l u_l)_H}{(\rho_l u_l)_A}\left[\left(\frac{\gamma + 3}{\gamma - 1}\right)_H\left(\frac{\gamma - 1}{\gamma + 3}\right)_A\right]^{1/2} \tag{72}$$

This transformation changes the value of 1.061 to 0.847. This latter value is in essential agreement with the value of 0.860 obtained by use of the results of reference 33 (eq. (70)). Note that for simulation of local mass flows $(p_{max}\rho_{max})_H$ must be less than $(p_{max}\rho_{max})_A$; for simulation at the sonic point $\frac{(p_{max}\rho_{max})_H}{(p_{max}\rho_{max})_A}$ must be about 0.89 (from eq. (71)).

Induced pressures and shock shape from leading-edge blunting.- In reference 34 the downstream influence of a two-dimensional blunt leading edge in inviscid hypersonic flow has been derived by use of first-order planar-blast-wave theory. The constants in the equations for the induced pressure and shock shape are given for air and helium. From these results the condition for the induced pressures to be the same, that is, for $\left(\frac{\Delta p}{p_1}\right)_H$ to equal $\left(\frac{\Delta p}{p_1}\right)_A$, is

$$\left[0.169 C_D^{2/3} M_1^2 \left(\frac{x}{t}\right)^{-2/3}\right]_H = \left[0.112 C_D^{2/3} M_1^2 \left(\frac{x}{t}\right)^{-2/3}\right]_A \qquad (73)$$

where t is the leading-edge thickness and C_D is the nose drag coefficient. In the following example the leading edge may be taken to be of any shape so long as its drag coefficient may be represented as the product of $C_{p,max} = \frac{\gamma + 3}{\gamma + 1}$ and some factor that is a function of shape only $\left(\text{e.g., for a flat-face leading edge } C_D \text{ may be taken as } \frac{\gamma + 3}{\gamma + 1}; \text{ for a cylindrical leading edge } C_D \approx \frac{2}{3}\frac{\gamma + 3}{\gamma + 1}\right)$. For this family of two-dimensional leading edges, equation (73) yields as the simulation requirement

$$\frac{M_{1,H}}{M_{1,A}}\left[\frac{\left(\frac{x}{t}\right)_A}{\left(\frac{x}{t}\right)_H}\right]^{1/3} = 0.827 \qquad (74)$$

The three variables involved offer several approaches for simulation. For example, if $M_{1,H} = M_{1,A}$ and $t_H = t_A$, then $x_H = 1.77x_A$; in helium a given induced pressure $\Delta p/p_1$ from leading-edge blunting will occur at a station that is farther rearward than it is in air. In order for the same induced pressure $\Delta p/p_1$ to occur at the same downstream station, t_H must equal $0.566t_A$. For the same station and free-stream Mach number

equation (73) shows that $\left(\frac{\Delta p}{p_1}\right)_H$ is 1.44 times $\left(\frac{\Delta p}{p_1}\right)_A$, whereas, for the same value of the parameter $\left(M_1^3 C_D \frac{t}{x}\right)$, the value of $\left(\frac{\Delta p}{p_1}\right)_H$ is 1.51 times the value of $\left(\frac{\Delta p}{p_1}\right)_A$. This latter result is in reasonable agreement with results for sonic-wedge leading edges obtained by the rotational-characteristics calculations of references 16 and 35. (Recall that blast-wave theory does not apply very near the leading edge nor very far downstream, but in the intervening region.) Reference 35 shows that an improvement on the first-order blast-wave theory prediction of the induced pressures is obtained by subtracting an empirical constant of 0.2. However, since this constant is found to be the same for helium and air, it does not affect equation (73) or the results derived therefrom.

From reference 34 the condition for the shock shape created by leading-edge blunting to be the same in helium and air $\left(\text{i.e.}, \left(\frac{y}{x}\right)_H = \left(\frac{y}{x}\right)_A\right)$ is

$$\left[0.90 C_D^{1/3} \left(\frac{x}{t}\right)^{2/3}\right]_H = \left[0.73 C_D^{1/3} \left(\frac{x}{t}\right)^{2/3}\right]_A \qquad (75)$$

This expression includes a correction by Cheng to the constant for air (0.73 instead of 0.89 as given in ref. 34). For the same family of leading edges mentioned in connection with equation (74), there is obtained $\left(\frac{x}{t}\right)_H \approx \frac{3}{4}\left(\frac{x}{t}\right)_A$; thus, for the shock shape in helium to be coincident with that in air, t_H must be about $1.33 t_A$. For the same value of the parameter $C_D\left(\frac{x}{t}\right)^2$, the value of $\left(\frac{y}{x}\right)_H$ is $1.23\left(\frac{y}{x}\right)_A$. Note that these results apply to the aforementioned intervening region and that as x becomes large the effects of γ must disappear since in the limit the shock attenuates to a Mach wave.

Because of the inadequacy of blast-wave theory very near the leading edge, other approximations of the pressure on the surface immediately after the juncture of a sonic wedge with a flat plate and of a sonic cone with a cylinder are of interest. An expression is given in reference 35 for this so-called shoulder pressure for the sonic-wedge—plate in air and in helium. These results may be used to show that for $M_1 \gg 1$ the ratio of $\left(\frac{\Delta p}{p_1}\right)_H$ to $\left(\frac{\Delta p}{p_1}\right)_A$ at the shoulder is 1.095. Calculations of

a similar nature have been made for the sonic-cone—cylinder, and in this case the ratio of $\left(\frac{\Delta p}{p_1}\right)_H$ to $\left(\frac{\Delta p}{p_1}\right)_A$ at the shoulder for $M_1 \gg 1$ is found to be about 1.012. This lower ratio for the sonic cone as compared with the sonic wedge is associated with the greater expansion angle that the flow experiences at the cone shoulder as compared with the wedge shoulder. In this regard, note that the limiting value of $\frac{\Delta p}{p_1}$ through an expansion to a vacuum is -1; therefore, the limiting ratio of $\left(\frac{\Delta p}{p_1}\right)_H$ to $\left(\frac{\Delta p}{p_1}\right)_A$ is unity. The ratio for the sonic cone must therefore lie between the sonic-wedge value of 1.095 and the limiting value of unity; it is found to lie close to the latter.

In reference 36, the pressure distribution over the cylindrical afterbody of a hemisphere-cylinder in air is given by blast-wave theory as

$$\left(\frac{p}{p_1}\right)_A = \frac{0.133M^2}{x/r} + 0.405 \tag{76}$$

where r is the radius of curvature of the nose and x is distance along the body surface measured from the forward stagnation point. Unpublished results of a general study of bodies of revolution with sonic or near-sonic tips by Mr. Vernon Van Hise of the Langley Research Center indicate that at a given body station over that portion of the body where blast-wave theory may be expected to apply, the induced pressure in helium may be expressed to first order, at least, by

$$\left(\frac{\Delta p}{p_1}\right)_H = (\text{Constant})\left(\frac{\Delta p}{p_1}\right)_A \tag{77}$$

where the constant of proportionality is of the order of $5/4$. On the assumption that this result is indicative of what may be expected for a hemisphere-cylinder, it follows that for $M_{1,H} = M_{1,A}$ and the same induced pressure in air and helium,

$$\left(\frac{x}{r}\right)_H \approx \frac{5}{4}\left(\frac{x}{r}\right)_A \tag{78}$$

Thus, the results for the axisymmetric case agree qualitatively with the two-dimensional results. A difference in pressure decay between planar flow and axisymmetric flow is, of course, to be expected.

Prandtl-Meyer flow.- Although the low-pressure sides of airfoils and bodies at hypersonic speeds are generally of secondary interest, Prandtl-Meyer expansive flow continues to have a number of useful applications in hypersonic aerodynamics (e.g., in the flow over curved nose shapes, such as ogives). Some aspects of Prandtl-Meyer flow pertinent to air-helium simulation will therefore be presented.

The results of references 37 to 39 show that for $M_1 \gg 1$ and an isentropic expansion from M_1 to M_f

$$\Delta\nu = \frac{2}{\gamma - 1}\left(\frac{1}{M_1} - \frac{1}{M_f}\right) \tag{79}$$

where $\Delta\nu$ is the expansion angle from M_1 (i.e., $\nu_f - \nu_1$). (Note that M_1 is not restricted to free-stream usage but may be the value of M at any point so long as the ensuing expansion is isentropic.) If $M_{1,H} = M_{1,A}$, then for $M_{f,H}$ to equal $M_{f,A}$ there is obtained

$$\frac{(\Delta\nu)_H}{(\Delta\nu)_A} = \frac{\gamma_A - 1}{\gamma_H - 1} = 0.60 \tag{80}$$

This result is compatible with one of the well-known advantages pointed out at the beginning of this paper for hypersonic helium tunnels, namely, that less expansion is required to reach a given hypersonic Mach number with helium than with air.

For $M_1 \gg 1$, it may be also shown that

$$\frac{p_f}{p_1} = \left(\frac{M_1}{M_f}\right)^{\frac{2\gamma}{\gamma-1}} \tag{81}$$

One interesting result of this relation is that if $\left(\frac{M_1}{M_f}\right)_H = \left(\frac{M_1}{M_f}\right)_A$, then

$$\frac{\left(\frac{p_f}{p_1}\right)_H}{\left(\frac{p_f}{p_1}\right)_A} = \left(\frac{M_1}{M_f}\right)^{\frac{2\gamma_H}{\gamma_H-1} - \frac{2\gamma_A}{\gamma_A-1}} = \left(\frac{M_f}{M_1}\right)^2 \tag{82}$$

The pressure coefficient for an expansion of $\Delta\nu$ is, for $M_1 \gg 1$, given by

$$C_p = \frac{2}{\gamma M_1^2}\left[\left(1 - \frac{\gamma - 1}{2} M_1 \Delta\nu\right)^{\frac{2\gamma}{\gamma-1}} - 1\right] \tag{83}$$

In order to examine under what conditions $C_{p,H} = C_{p,A}$, some additional basic differences between expansions in air and helium must be considered. Equations (79) to (82) have already implied that the pressure drop through a given expansion angle $\Delta\nu$ is, for $M_1 \gg 1$, greater in air than in helium. Thus, $\Delta\nu$ in helium will need to be greater than $\Delta\nu$ in air to achieve simulation of C_p. But recall that the maximum value of $\Delta\nu$ (expansion from $M_1 = 1$ to $M_1 = \infty$) is

$$\Delta\nu_{max} = 90^\circ\left(\sqrt{\frac{\gamma + 1}{\gamma - 1}} - 1\right) \tag{84}$$

which shows that the maximum expansion angle in helium is only about 0.69 times that in air. Furthermore, in expanding to a vacuum, the ratio of $C_{p,H}$ to $C_{p,A}$ for $M_{1,H} = M_{1,A}$ is equal to γ_A/γ_H or 0.84. Thus, it is impossible to simulate in helium expansion angles that are as large as, or pressure coefficients that are as low as, those that can be reached in air. (Fortunately these extreme conditions play, with few exceptions, a negligible role in hypersonic aerodynamics.) The minimum value of $C_{p,A}$ that can be simulated is $-\frac{2}{\gamma_H M_{1,H}^2}$. The maximum value of $\Delta\nu_A$ that can be simulated can therefore be determined, with the aid of equation (83), from

$$-\frac{2}{\gamma_H M_{1,H}^2} = \frac{2}{\gamma_A M_{1,A}^2}\left[\left(1 - \frac{\gamma_A - 1}{2} M_{1,A} \Delta\nu_A\right)^{\frac{2\gamma_A}{\gamma_A-1}} - 1\right] \tag{85}$$

For $M_{1,H} = M_{1,A}$ the following equation is obtained for the maximum value for $\Delta\nu_A$ that can be simulated in helium:

$$\Delta\nu_{A,max} = -\frac{1}{M_{1,A}}\left(\frac{2}{\gamma_A - 1}\right)\left[\left(1 - \frac{\gamma_A}{\gamma_H}\right)^{\frac{\gamma_A-1}{2\gamma_A}} - 1\right] \tag{86}$$

This equation yields

$$\Delta\nu_{A,max} = \frac{1.152}{M_{1,A}} \tag{87}$$

This expression gives good results; for example, at $M_{1,A} = 10$ it gives $\Delta\nu_{A,max} = 6.60^{\circ}$ as compared with the exact value of 6.54°.

The general condition for $C_{p,H} = C_{p,A}$ is, from equation (83), given by (for $M_{1,H} = M_{1,A}$)

$$K_H = \frac{2}{\gamma_H - 1}\left\{1 - \left[\frac{\gamma_H}{\gamma_A}\left(1 - \frac{\gamma - 1}{2}K\right)_A^{\frac{2\gamma_A}{\gamma_A - 1}} - \frac{\gamma_H}{\gamma_A} + 1\right]^{\frac{\gamma_H - 1}{2\gamma_H}}\right\} \tag{88}$$

where K is the hypersonic similarity parameter and equals $M_1 \Delta\nu$ in this case. From equation (87) the maximum value of K_A that can be simulated is 1.152. The following table lists values of K_H/K_A for $C_{p,H} = C_{p,A}$ as a function of K_A:

K_A	K_H/K_A
0	1
.2	1.01
.4	1.04
.6	1.08
.8	1.14
1.0	1.29
1.152	2.60

The value of $K_H/K_A = 2.60$, corresponding to the minimum value of $C_{p,A}$ that can be simulated $\left(\text{i.e., } C_{p,A} = C_{p,H} = -\frac{2}{\gamma_H M_{1,H}^2}\right)$, is in excellent agreement with exact results for $M_1 \gg 1$. For example, with $M_{1,H} = M_{1,A}$ exact calculations give $\left(\frac{\Delta\nu_H}{\Delta\nu_A}\right)_{max} = 2.60$ at $M_1 = 10$; at $M_1 = 1.5$ the

exact value has decreased to only 2.53. With regard to this latter value, the value of M at the match point[11] on rounded blunt noses is about 1.5.

Lift-drag ratio.- The identical form of equations (27) and (39) implies that, at least for simple shapes like the flat plate and wedge, the value of lift-drag ratio at small angles of attack is essentially the same in helium and air. Thus, the maximum lift-drag ratios should be essentially the same. An implicit indication of the lack of γ effects upon L/D for slender shapes at low angles of attack also exists in the following series expression for weak shock waves:

$$C_p = \left[\frac{2}{\left(M_1^2 - 1\right)^{1/2}}\right]\delta + \left[\frac{(\gamma + 1)M_1^4 - 4\left(M_1^2 - 1\right)}{2\left(M_1^2 - 1\right)^2}\right]\delta^2 + \ldots \qquad (89)$$

For $\delta \ll 1$ and $M_1 \gg 1$, this expression shows that the value of $\frac{dC_p}{d\delta}$ is $2/M_1$ and is therefore unaffected by γ.

Figure 14 shows exact calculations of lift coefficient, drag coefficient, and lift-drag ratio for an asymmetric wedge at $M_1 = 20$ in air and helium. The curves for lift-drag ratio in air and helium are almost the same.

Closing comments on simulation in inviscid flows.- The preceding results have illustrated that the differences between air and helium may be easily evaluated and that the simulation conditions may be expressed in simple form, at least for simulation of the parameters that have been examined. There are other facets of air-helium simulation not included herein that have been treated in previous studies (e.g., the free-jet-simulation studies of refs. 40 to 42), and there are many aspects that remain to be examined. However, as stated at the outset, it is not within the scope or intent of this paper to attempt an exhaustive treatment but rather to compile the results of some recent examinations with the idea that these results are illustrative of what can be attempted in hypersonic studies in helium. With this view, inviscid flows will not be considered further, and attention will be turned to viscous flows.

---

[11]Point on nose where blunt-nose modified Newtonian theory is matched to Prandtl-Meyer theory in order to improve the prediction at large values of φ.

Viscous Flow

Remarks on viscosity laws.- For approximations of skin-friction coefficient at moderate temperatures in helium, a value of $\omega_H = 0.75$ is sometimes used for the exponent in the power law for viscosity. This value agrees closely with the value of $\omega_A = 0.76$ which gives good results for air in the temperature range of about 300° to 900° R and serves as a fair approximation for a somewhat wider range of temperatures. Thus, an assumption of $\omega_H = \omega_A$ may be sufficiently accurate under certain conditions. However, when high temperatures are involved, the power law for air becomes increasingly inaccurate with increasing temperature unless ω_A is varied. (See ref. 43, e.g.) Of course, for best accuracy in air, Sutherland's law is to be preferred. The results of reference 12 show that the power law gives good results for helium (better than Sutherland's law) over a wide range of temperatures and that for best results the value of ω_H should be 0.647 instead of 0.75. For these reasons, it is desirable to include in the examinations of skin-friction simulation the effects of the use of different viscosity laws.

Development of simulation conditions for average flat-plate skin-friction coefficient.- The reference-temperature method (see ref. 44) will be employed with T^* denoting the reference temperature and T_1 the free-stream temperature.

The average skin-friction coefficient may be expressed as (refs. 37 and 43)

$$C_F = K_i \frac{\left(\frac{T_1}{T^*}\right)^{1-N}\left(\frac{\mu^*}{\mu_1}\right)^N}{R^N} \tag{90}$$

where K_i is the constant in the incompressible skin-friction laws and N is the Reynolds number exponent in the same laws (in this paper $N = 1/2$ for laminar flow and $N = 1/5$ for turbulent flow).

If the power law for viscosity

$$\frac{\mu^*}{\mu_1} = \left(\frac{T^*}{T_1}\right)^{\omega} \tag{91}$$

is used for both helium and air, then the general expression for simulation with $R_H = R_A$ is

$$\frac{C_{F,H}}{C_{F,A}} = \frac{\left(\frac{T_1}{T^*}\right)_H^{1-N-N\omega_H}}{\left(\frac{T_1}{T^*}\right)_A^{1-N-N\omega_A}} \tag{92}$$

If Sutherland's law

$$\frac{\mu^*}{\mu_1} = \left(\frac{T^*}{T_1}\right)^{3/2} \frac{1 + \frac{\beta}{T_1}}{\frac{T^*}{T_1} + \frac{\beta}{T_1}} \tag{93}$$

is used for air and the power law is used for helium, then the general expression for simulation with $R_H = R_A$ is

$$\frac{C_{F,H}}{C_{F,A}} = \frac{\left(\frac{T_1}{T^*}\right)_H^{1-N-N\omega_H}}{\left(\frac{T_1}{T^*}\right)_A^{1-\frac{5N}{2}} \left(\frac{1 + \frac{\beta}{T_1}}{\frac{T^*}{T_1} + \frac{\beta}{T_1}}\right)_A^N} \tag{94}$$

There are several proposed expressions for T^*/T_1 (see ref. 43, e.g.), a number of which give essentially the same results, particularly for $M_1 \gg 1$. The following expression from reference 45 will be used in the examples herein and corresponds to an insulated plate and a Prandtl number of unity:

$$\frac{T^*}{T_1} = 1 + 0.727 \frac{\gamma - 1}{2} M_1^2 \tag{95}$$

Results for $C_{F,H} = C_{F,A}$ and $R_H = R_A$.- Four conditions were selected for calculating the ratio $M_{1,H}/M_{1,A}$ for simulation (insulated plate, $N_{Pr} = 1$). These were $\omega_H = \omega_A = 0.76$ (by eq. (92)); $\omega_A = 0.76$ and $\omega_H = 0.647$ (by eq. (92)); $\omega_H = 0.647$ and values of $\beta_A/T_{1,A}$ representative of an air wind tunnel (by eq. (94)); and $\omega_H = 0.647$ and values of $\beta_A/T_{1,A}$ representative of those encountered by a rocket

glider in its glide trajectory (by eq. (94)). It is important to note that the flight example establishes only the effects of flight values of $\beta_A/T_{1,A}$ for the case of an insulated plate. The effects of the large and unavoidable heat transfer in actual flight might be overriding. This case has not been examined; however, if equation (95) is generalized to include heat transfer this problem is readily attacked.

In order to obtain the values of $\beta_A/T_{1,A}$ for the wind-tunnel illustration, a value of stagnation pressure was assigned to a given value of $M_{1,A}$, and a value of $T_{1,A}$ slightly above the theoretical value for condensation was determined from these conditions (unless the stagnation temperature would be less than 100° F, which was fixed as a lower limit). A few of these selected values of stagnation pressure are given in the following table with the values of $T_{1,A}$:

$M_{1,A}$	p_t, lb/sq in. abs	$T_{1,A}$, °R
4	200	133
6	600	100
12	4,500	90
22	20,000	80

A value of β_A of 198 was used to obtain the values of $\beta_A/T_{1,A}$. At extremes of temperature there may be some justification for using values of β_A different from 198; however, the value of about 198 is known to be adequate, at least for temperatures between 150° and 3,300° R (see ref. 43, e.g.) and probably for considerably higher temperatures. Furthermore, for the case of the air wind tunnel of this example where values of $T_{1,A}$ about 100° R are indicated, the use of a more accurate value of β_A for these low temperatures ($\beta_A \approx 180$) has only a minor effect on the results. For this example, then, the values of $\beta_A/T_{1,A}$ are of the order of 2 to 2.5 at hypersonic speeds.

In order to establish the flight values of $\beta_A/T_{1,A}$, a rocket glider was assumed to be following a reentry glide path at a constant lift coefficient of 0.06 with a wing loading of 20 $\left(\text{e.g., to be gliding at constant } \frac{C_L}{W/S} \text{ of } 0.003\right)$. This flight path corresponds approximately to a speed range of $M_{1,A} = 26$ down to $M_{1,A} = 1$ as the glider descends from about 250,000 feet to about 50,000 feet. The values of $\beta_A/T_{1,A}$ for this glide path under free-air conditions are shown in figure 15 and may be observed to range between about 0.39 to 0.56. It is interesting to

observe that these values of $\beta_A/T_{1,A}$ are very near the value of 0.505 generally used in Sutherland's law for free-air conditions at the lowest isothermal altitude. (A comparison between experimental viscosity results and Sutherland's law for $\frac{\beta_A}{T_{1,A}} = 0.505$ may be seen in ref. 43.)

The values of $M_{1,H}/M_{1,A}$ for the four conditions that were selected for examination are shown as a function of $M_{1,A}$ for laminar flow ($N = 1/2$) in figure 16(a). For $\omega_H = \omega_A$ (independent of the value of ω) equation (92) yields[12]

$$\frac{M_{1,H}}{M_{1,A}} = \sqrt{\frac{\gamma_A - 1}{\gamma_H - 1}} = 0.775 \tag{96}$$

Figure 16(a) shows this result to differ considerably from the other results that make use of more accurate viscosity relations. The use of $\omega_A = 0.76$ and $\omega_H = 0.647$ gives a curve that approaches good agreement with that given for the air-wind-tunnel values of $\beta_A/T_{1,A}$ for $M_{1,A} \gg 1$. It is important to note the wide difference in the values of $M_{1,H}/M_{1,A}$ at hypersonic speeds between flight and wind-tunnel values of $\beta_A/T_{1,A}$; for $M_{1,A} \gg 1$, values of $M_{1,H}/M_{1,A}$ of the order of 0.3 to 0.4 are required for the example of wind-tunnel simulation, whereas for the flight example the values of $M_{1,H}/M_{1,A}$ are not greatly different from unity.

For the turbulent boundary ($N = 1/5$) figure 16(b) shows that all four conditions examined give values of $M_{1,H}/M_{1,A}$ that are of the same general magnitude and that are relatively insensitive to changes in $M_{1,A}$. For $M_{1,A} \gg 1$, the values of $M_{1,H}/M_{1,A}$ range from about 0.7 for the wind-tunnel example to about 0.8 for the flight example. Thus, although inadequate for laminar flow, equation (96) may be satisfactory for turbulent flow. It remains, however, to interpret the importance of differences in $M_{1,H}/M_{1,A}$ in terms of differences in $C_{F,H}/C_{F,A}$, for as was shown in the section on inviscid simulation, large differences between the values of $M_{1,H}$ and $M_{1,A}$ required for simulation do not necessarily imply that large differences exist without simulation for the parameter in question. With this in mind, an examination has been made in the following section of the difference that exists between $C_{F,H}$ and $C_{F,A}$ when the Mach number and Reynolds number are the same in air and in helium.

---

[12]This result has been previously obtained by Fred W. Matting and Dean R. Chapman of the Ames Research Center, NASA, for both laminar and turbulent boundary layers.

Results for $M_{l,H} = M_{l,A}$ and $R_H = R_A$.- The curves of figure 17(a) for laminar flow show, by comparison with the curves of figure 16(a), that the deviations from unity in the values of $M_{l,H}/M_{l,A}$ that are required for simulation do not imply equally large deviations from unity in the values of $C_{F,H}/C_{F,A}$ without simulation. Without simulation (fig. 17(a)) the values of $C_{F,H}$ for the flight example are within 10 percent or less of the values of $C_{F,A}$ over the entire Mach number range, and for $M_l \gtrsim 12$ they are within 2 or 3 percent. Also without simulation, the values of $C_{F,H}/C_{F,A}$ for the wind-tunnel example and for the power-law curve with $\omega_A = 0.76$ and $\omega_H = 0.647$ come into close agreement at the higher Mach numbers and tend toward a value near 0.7. Figure 17(a) also shows that the least-accurate assumption of $\omega_A = \omega_H = 0.76$ (eq. (96)) leads to values for $C_{F,H}/C_{F,A}$ not greatly different from unity; $C_{F,H}$ is only about 6 percent less than $C_{F,A}$ for $M_l \gtrsim 8$.

The curves of figure 17(b) for turbulent flow show, by comparison with the curves of figure 16(b), that the deviations from unity in the values of $M_{l,H}/M_{l,A}$ that are required for simulation are, at hypersonic speeds, indicative of the deviations from unity in the values of $C_{F,H}/C_{F,A}$ without simulation. For turbulent flow, the relative insensitiveness of the results to the viscosity law employed and to the value of $T_{l,A}$ is also evident. Thus, for turbulent flow the assumption of $\omega_A = \omega_H$ (eq. (96)) may give a reasonable approximation; it gives results within a few percent of the results for the flight example.

Hypersonic approximations of results for $R_H = R_A$.- For the results presented thus far (case of $\omega_H = \omega_A$ excluded, eq. (96)), the following expressions may be used for $M_l \gtrsim 10$. All these expressions are for an insulated plate, Prandtl number of unity, and $R_H = R_A$.

(1) Power law for helium and air ($\omega_A = 0.76$; $\omega_H = 0.647$)

(a) Laminar flow ($N = 1/2$):

For $C_{F,H} = C_{F,A}$,

$$\frac{M_{l,H}}{M_{l,A}} = 1.05 M_{l,A}^{-0.32} \tag{97}$$

For $M_{1,H} = M_{1,A}$,

$$\frac{C_{F,H}}{C_{F,A}} = 1.02M_1^{-0.11} \tag{98}$$

(b) Turbulent flow (N = 1/5):

For $C_{F,H} = C_{F,A}$,

$$\frac{M_{1,H}}{M_{1,A}} = 0.80M_{1,A}^{-0.034} \tag{99}$$

For $\dot{M}_{1,H} = M_{1,A}$,

$$\frac{C_{F,H}}{C_{F,A}} = 0.74M_1^{-0.045} \tag{100}$$

Note the similarity of equations (99) and (100) which supports the conclusion of the preceding section that values of $M_{1,H}/M_{1,A}$ are indicative of the values of $C_{F,H}/C_{F,A}$ if the flow is turbulent.

(2) Sutherland's law for air; power law for helium ($\omega_H = 0.647$)

(a) Laminar flow (N = 1/2):

For $C_{F,H} = C_{F,A}$,

$$\frac{M_{1,H}}{M_{1,A}} = 0.52M_{1,A}^{0.42}\left(\frac{1}{1 + \frac{\beta_A}{T_{1,A}}}\right)^{1.42} \tag{101}$$

For $M_{1,H} = M_{1,A}$,

$$\frac{C_{F,H}}{C_{F,A}} = 0.79M_1^{0.15}\left(\frac{1}{1 + \frac{\beta_A}{T_{1,A}}}\right)^{0.50} \tag{102}$$

(b) Turbulent flow ($N = 1/5$):

For $C_{F,H} = C_{F,A}$,

$$\frac{M_{l,H}}{M_{l,A}} = 0.75 M_{l,A}^{0.044} \left(\frac{1}{1 + \frac{\beta_A}{T_{l,A}}} \right)^{0.15} \tag{103}$$

For $M_{l,H} = M_{l,A}$,

$$\frac{C_{F,H}}{C_{F,A}} = 0.67 M_l^{0.059} \left(\frac{1}{1 + \frac{\beta_A}{T_{l,A}}} \right)^{0.20} \tag{104}$$

L
4
1
4

Simulation of C_F for $M_{l,H} = M_{l,A}$ by use of Reynolds number.- Although the use of the Mach number ratio to achieve skin-friction simulation is suitable for some types of investigations, the wide difference in Mach numbers between helium and air that may be involved would be undesirable in many studies, particularly those in which the objective is to simulate, insofar as possible, nonviscous and viscous effects simultaneously. In such tests the condition $M_{l,H} = M_{l,A}$ would, in general, be preferred in view of the inviscid-simulation requirements shown in this paper.

With the results that have been presented for $C_{F,H}/C_{F,A}$ with $M_{l,H} = M_{l,A}$ and $R_H = R_A$, the ratio of R_H/R_A necessary for $\frac{C_{F,H}}{C_{F,A}} = 1$ with $M_{l,H} = M_{l,A}$ may be established as follows.

Let $\sigma \equiv \frac{C_{F,H}}{C_{F,A}}$ for $R_H = R_A$. With the aid of equation (90), the following expression is obtained:

$$\frac{C_{F,H}}{C_{F,A}} = 1 = \sigma \left(\frac{R_A}{R_H} \right)^N \tag{105}$$

It follows that for laminar flow (with $N = 1/2$)

$$\frac{R_H}{R_A} = \sigma^2 \tag{106}$$

and for turbulent flow (with $N = 1/5$)

$$\frac{R_H}{R_A} = \sigma^5 \tag{107}$$

Thus, equations (106) and (107) in conjunction with figures 17(a) and 17(b), or the results of the preceding section, permit the determination of the value of R_H/R_A for simulation of C_F with $M_{1,H} = M_{1,A}$.

For example, take $M_1 = 20$ and $R_A = 10 \times 10^6$. For the air-wind-tunnel simulation example, there is obtained $R_H = 4.65 \times 10^6$ for laminar flow and 4.01×10^6 for turbulent flow. For the flight example, $R_H = 10.57 \times 10^6$ for laminar flow and 5.55×10^6 for turbulent flow. Thus, the wind-tunnel example requires approximately the same value of R_H for laminar and turbulent flow, while the flight example requires what may be significantly different values of R_H for laminar and turbulent flow. Such factors as these will determine whether it is more attractive to obtain first an air simulation for wind-tunnel conditions and then convert these results to flight values or to simulate flight conditions directly. The amount of laminar or turbulent flow that may be expected on a vehicle would also enter into the decision.

Effect of Mach number on skin-friction coefficient in helium.- The variation of C_F in helium with M_1 may be obtained by use of equations (90) and (95), or the simulation results that have been derived may be used to transform a base curve for air. The latter approach has been used herein to afford a direct comparison between the air curve and the helium curve and to demonstrate the application of the simulation results. Either the ratio $C_{F,H}/C_{F,A}$ or $M_{1,H}/M_{1,A}$ may be used in the transformations.

For laminar flow, figure 18, Sutherland's formula with $\frac{\beta_A}{T_{1,A}} = 0.505$ has been used in equation (90) to obtain the base curve for air. This curve is in essential agreement with the Crocco solution at the same Prandtl number. Small differences in Prandtl number are of minor importance, however, since, as has been shown in references 46 and 47, variations in Prandtl number, at least within the range $0.725 \leqq N_{Pr} \leqq 1.0$, have only minor effects on the values of C_F. (Also compare the present air curve with the Crocco solution in ref. 43 for which $N_{Pr} = 0.725$.) Because of the sensitiveness of the laminar simulation results to the viscosity law employed and to the value of $\beta_A/T_{1,A}$, transformation of this particular air curve must be restricted to values of $\beta_A/T_{1,A}$

near 0.505 and to use of Sutherland's law for air. Consequently, the flight example of this paper has been used to obtain the helium curve in figure 18.

For turbulent flow, the simulation results are relatively insensitive to the viscosity law employed and to the value of $\beta_A/T_{1,A}$; consequently, the power law with $\omega_A = 0.76$ has been used in equation (90) to obtain the base curve for air shown in figure 19. This curve gives slightly lower values of $C_F/C_{F,i}$ than those given by the Van Driest solution (ref. 47) that employs the power law for viscosity and the similarity law for mixing length; however, this base curve appears to be in close agreement with experimental results for zero heat transfer shown in reference 37. Since the power law has been used for the air curve, the power-law simulation results (with $\omega_A = 0.76$ and $\omega_H = 0.647$) have been used in the transformation of the air curve to obtain the helium curve in figure 19.

Although the value of 0.76 for ω_A that has been used in the examples herein gives good results for moderate temperature applications, a change in temperature level at a given reference-temperature ratio may significantly change the value of ω_A, as shown in figure 20. Such changes in ω_A are more important for laminar flows than for turbulent flows, both with regard to the skin-friction coefficients and the simulation ratios. For example, the results shown in figures 16 and 17 imply that large changes in ω_A have a minor effect on the simulation ratios for turbulent flow.

Simulation of displacement thickness.- The displacement thickness of the boundary layer can be of considerable importance at hypersonic speeds, and its treatment in the literature has been extensive. It will only be noted here that when the skin-friction coefficient is simulated, the boundary layers are similar for practical purposes, and the displacement thickness is therefore simulated. For example, take the case of $M_1 \gg 1$ and an insulated plate with $N_{Pr} = 1$. For simplicity, take the simplest viscosity assumption used previously, that is, $\omega_H = \omega_A$. (Note that, as before, this is not the best assumption, but it is sufficient for this purpose.) For these conditions the displacement thickness is given by (ref. 37, e.g.)

$$\frac{\delta^*}{l} \approx (\gamma - 1)\frac{M_1^2}{R^N} \tag{108}$$

from which the displacement thickness in helium is indicated to be 5/3 times that in air for the same values of M_1 and R^N. For simulation of δ^* with $R_H = R_A$, equation (108) yields the same ratio of $M_{1,H}/M_{1,A}$ as that given by equation (96) for simulation of skin-friction coefficient under the same initial assumptions.

Boundary-layer displacement effects, weak interaction.- From reference 48 the first approximation to the pressure distribution that is induced by the presence of the laminar boundary layer on a flat plate with sharp leading edge (Prandtl number of unity) is, in the weak interaction region, given by

$$\frac{\Delta p}{p_1} = \gamma M_1 \delta_e \tag{109}$$

where in this case δ_e is the flow deflection angle at the edge of the boundary layer and is given by

$$\delta_e = \zeta M_1^2 \sqrt{\frac{C}{R}} = \frac{\zeta}{M_1} \bar{\chi} \tag{110}$$

In this expression $\bar{\chi}$ is the interaction parameter $\frac{M_1^3 \sqrt{C}}{\sqrt{R}}$, where R is based on distance along the surface from the leading edge and C is the constant of proportionality in the linear form of the temperature-viscosity relation $\frac{\mu^*}{\mu_1} = C \frac{T^*}{T_1}$. For the insulated plate, $\zeta = 0.599(\gamma - 1)$, and for the noninsulated highly cooled plate, with $M_1 \to \infty$, $\zeta = 0.166(\gamma - 1)$. For simulation of δ_e for either the insulated or noninsulated plate, the ratio of the interaction parameters must therefore be, for $M_{1,H} = M_{1,A}$,

$$\frac{\bar{\chi}_H}{\bar{\chi}_A} = \frac{\gamma_A - 1}{\gamma_H - 1} = 0.60 \tag{111}$$

This result[13] may be used with equation (109) to show that simulation of $\Delta p/p_1$ with $M_{1,H} = M_{1,A}$ requires

$$\frac{\bar{\chi}_H}{\bar{\chi}_A} = \frac{\gamma_A}{\gamma_H}\left(\frac{\gamma_A - 1}{\gamma_H - 1}\right) = 0.50 \tag{112}$$

The derivations in reference 48 imply that equations (111) and (112) apply so long as the ratio of the wall temperature to free-stream stagnation temperature is essentially the same in helium and air.

---

[13]From reference 48 the ratio of the boundary-layer thickness to distance from the leading edge, for $M_1 \gg 1$, is in the weak interaction region $\frac{0.332(\gamma - 1)\bar{\chi}}{M_1}$. Equation (111) is thus the simulation condition for this ratio as well as for δ_e.

A simulation condition for $M_{1,H} = M_{1,A}$ that is represented by $\bar{\chi}_H/\bar{\chi}_A$ may be expressed in terms of the Reynolds number requirement for simulation by

$$\frac{R_H}{R_A} = \frac{C_H}{C_A}\left(\frac{\bar{\chi}_H}{\bar{\chi}_A}\right)^{-2} \tag{113}$$

Values of C_H/C_A may, with the aid of equation (95), be determined from

$$C = \left(\frac{T^*}{T_1}\right)^{\omega-1} \tag{114}$$

for the power law for viscosity and

$$C = \left(\frac{T^*}{T_1}\right)^{1/2} \frac{1 + \frac{\beta}{T_1}}{\frac{T^*}{T_1} + \frac{\beta}{T_1}} \tag{115}$$

for Sutherland's law for viscosity. For example, with $M_1 \gg 1$, $\omega_A = 0.76$, and $\omega_H = 0.647$, the power law gives

$$\frac{C_H}{C_A} = \frac{1.04}{M_1^{0.226}} \tag{116}$$

If the results of other studies of the weak-interaction region are used to obtain the simulation requirements for $\left(\frac{\Delta p}{p_1}\right)_H = \left(\frac{\Delta p}{p_1}\right)_A$, the ratio of $\bar{\chi}_H/\bar{\chi}_A$ is found to be close to that given by equation (112). For example, the results of reference 49 yield $\bar{\chi}_H/\bar{\chi}_A = 0.50$, the results of reference 19 yield $\bar{\chi}_H/\bar{\chi}_A = 0.56$, and the results of reference 50 give $\bar{\chi}_H/\bar{\chi}_A = 0.52$.

Boundary-layer displacement effects, strong interaction.- From reference 51 (see also ref. 49) the induced pressure in the strong-interaction region on an insulated flat plate with sharp leading edge is given by

$$\frac{\Delta p}{p_1} = \gamma\left(\frac{\gamma - 1}{\gamma + 1}\right)^{1/2}\bar{\chi} - \frac{\gamma - 1}{\gamma + 1} - 1 \tag{117}$$

which yields as the simulation requirement for $\left(\frac{\Delta p}{p_1}\right)_H = \left(\frac{\Delta p}{p_1}\right)_A$

$$\frac{\bar{\chi}_H}{\bar{\chi}_A} = 0.685 + \frac{0.1}{\bar{\chi}_A} \tag{118}$$

In reference 52 the strong-interaction region has also been examined for an insulated flat plate for both a sharp and a blunt leading edge. The general expression for the induced pressure is (to first order) given in the form

$$\frac{\Delta p}{p_1} = A\bar{\chi}\left[1 + B\left(\frac{M_1\sqrt{C}}{\sqrt{R}}\right)^g\right] - 1 \tag{119}$$

The constants A, B, and g in this equation may be evaluated by the expressions in reference 52. The following results are obtained:

(1) For helium:

(a) Sharp leading edge

$$\frac{\Delta p}{p_1} = 0.92\bar{\chi}\left[1 + 1.78\left(\frac{M_1\sqrt{C}}{\sqrt{R}}\right)^{0.60}\right] - 1 \tag{120}$$

(b) Blunt leading edge

$$\frac{\Delta p}{p_1} = 0.92\bar{\chi}\left[1 + 2.18\left(\frac{M_1\sqrt{C}}{\sqrt{R}}\right)^{0.40}\right] - 1 \tag{121}$$

(2) For air:

(a) Sharp leading edge

$$\frac{\Delta p}{p_1} = 0.52\bar{\chi}\left[1 + 1.80\left(\frac{M_1\sqrt{C}}{\sqrt{R}}\right)^{0.524}\right] - 1 \tag{122}$$

(b) Blunt leading edge

$$\frac{\Delta p}{p_1} = 0.52\bar{\chi}\left[1 + 2.23\left(\frac{M_1\sqrt{C}}{\sqrt{R}}\right)^{0.286}\right] - 1 \tag{123}$$

For the zeroth-order solution the second term within the brackets in equations (120) to (123) becomes zero, and the solution is the same for the sharp and blunt leading edges. Thus, the zeroth-order simulation of $\Delta p/p_1$ requires that

$$\frac{\bar{X}_H}{\bar{X}_A} = 0.565 \tag{124}$$

The approximate agreement of this result for strong interaction with the results shown in the preceding section for weak interaction might be expected since if the pressures in the strong-interaction region are simulated, the pressures in the smoothly adjoining weak-interaction region should be reasonably simulated.

In order to examine the simulation requirements for the sharp and blunt leading edges according to equations (120) to (123), a range of values between 0 and 10 was selected for the parameter Z_A, where $Z \equiv \frac{M_1\sqrt{C}}{\sqrt{R}}$. This should give ample coverage of $\bar{X}$ for the present purposes (note $\bar{X} = M_1{}^2 Z$). The calculated ratios of Z_H/Z_A for simulation of $\Delta p/p_1$ are given in the following table for sharp and blunt leading edges:

Z_A	Z_H/Z_A	
	Sharp leading edge	Blunt leading edge
0	0.565	0.565
.0001	.570	.627
.001	.581	.662
.01	.605	.695
.1	.647	.695
.8	.664	.653
1.0	.663	.645
10	.625	.562

The value of $Z_A = 0.8$ is included in the table to show that $Z_A = 1.0$ is not associated with the maximum value of Z_H/Z_A for the sharp leading edge. This appears to be a trivial point, however, in view of the small variation of Z_H/Z_A with Z_A in the range of Z_A where strong-interaction theory should be most applicable, that is, $M_1{}^2 Z = \bar{X} \gg 1$.

Within the range $10^{-2} < Z_A < 1.0$, the values of Z_H/Z_A imply, for $M_1 \gg 1$, fair agreement with the values of $\bar{\chi}_H/\bar{\chi}_A$ given by equation (118). For values of Z_A much greater than 10 the value of Z_H/Z_A falls below that for $Z_A = 0$ (the zeroth-order approximation).

Note that the values of Z_H/Z_A given in the preceding table may be taken as values of $\bar{\chi}_H/\bar{\chi}_A$ if $M_{1,H} = M_{1,A}$. It follows that these values may be used with equations (113) through (116) if simulation by use of Reynolds number is desired.

The results of reference 18 may be used to show that equation (124), and therefore the values of Z_H/Z_A for simulation, are essentially independent of the ratio of wall temperature to recovery temperature. Relations given in reference 49 indicate that the ratios of $\bar{\chi}_H/\bar{\chi}_A$ for simulation of $\Delta p/p_1$ for both strong and weak interaction will also give simulation of the average (or local) skin-friction-drag coefficient that includes the displacement effect when the coefficient is expressed in the form $\dfrac{C_F\sqrt{R}}{\sqrt{C}}$.

The attention that has been given herein to displacement effects is not intended to imply that these effects will always play a major role in the pressure distribution. For example, when the wedge or cone angle downstream of a sharp or blunt leading edge is large, the displacement effects may be small (ref. 17), and the inviscid predictions are generally adequate.

Knudsen number and molecular speed ratio.- In tests at $M_1 \gg 1$ two parameters that may be of interest are the Knudsen number and the molecular speed ratio. The Knudsen number is given by

$$N_{Kn} = \frac{M_1}{R}\sqrt{\frac{\pi}{2}\gamma} \tag{125}$$

from which it follows that simulation of N_{Kn} by use of Reynolds number, with $M_{1,H} = M_{1,A}$, requires

$$\frac{R_H}{R_A} = \sqrt{\frac{\gamma_H}{\gamma_A}} = 1.091 \tag{126}$$

The molecular speed ratio is given by

$$N_\nu = M_1 \sqrt{\frac{\gamma}{2}} \tag{127}$$

and its simulation requires that

$$\frac{M_{1,H}}{M_{1,A}} = \sqrt{\frac{\gamma_A}{\gamma_H}} = 0.917 \tag{128}$$

which also achieves simulation of N_{Kn} if $R_H = R_A$.

Closing comments on simulation in viscous flows.- As for inviscid flows, a number of aspects of simulations of viscous flows remain to be examined, and extensions can be made to the work contained herein. For example, alternate forms of equation (95) that take into account heat transfer, varying specific heat, and varying Prandtl number will permit the simulation requirements to be established for these conditions. The method of similar solutions of the boundary-layer equations has been used in reference 18 to obtain the heat transfer, skin friction, and boundary-layer thickness in a pressure gradient for both air and helium; simulation conditions may be determined from these results for the family of pressure gradients considered. In establishing the conditions for simulation of heat transfer, gas properties other than γ must, of course, be considered (e.g., the properties involved in Prandtl number). In this regard, the difference in viscosity between air and helium has been indicated herein; the difference in conductivities is such that at room temperatures helium conducts heat almost seven times as fast as air; the difference in specific heats at constant pressure, also at room temperature, is such that pound for pound helium holds about five times as much heat as air. Additional details on the properties of helium and on operational problems involved in its use may be found in reference 15.

CONCLUDING REMARKS

The results of some studies of the air-helium simulation problem at hypersonic speeds have been compiled. The differences that may be expected between tests in air and tests in helium are illustrated, and simple expressions are presented for achieving simulation of a number of parameters. These simulation expressions are in most cases given in general form so that they may be applied to any two gases having different ratios of specific heat. An ideal gas has been assumed throughout. Both viscous and nonviscous flows are considered.

The results show that several parameters require the same conditions for simulation while other parameters require different conditions. Some parameters may not require simulation; a number have a value in helium that without simulation is within about 10 percent or less of the value in air; a few are negligibly different in air and helium. Thus, the overall results show that there is no general rule for air-helium simulation. Although complete simultaneous simulation of all flow conditions about a model will probably be rare, it does appear possible to obtain sufficient simulation for many types of aerodynamic as well as fluid-dynamic studies and to interpret most helium results in terms of air results.

Langley Research Center,
National Aeronautics and Space Administration,
Langley Field, Va., June 30, 1959.

REFERENCES

1. Bogdonoff, S. M., and Hammitt, A. G.: The Princeton Helium Hypersonic Tunnel and Preliminary Results Above M = 11. WADC Tech. Rep. 54-124, Wright Air Dev. Center, U.S. Air Force, July 1954.

2. Hammitt, A. G., and Bogdonoff, S. M.: A Study of the Flow About Simple Bodies at Mach Numbers From 11 to 15. Rep. No. 277 (Contract AF 33(038)-250), Princeton Univ., Aero. Eng. Lab., Sept. 1954.

3. Bogdonoff, Seymour M., and Hammitt, Andrew G.: Fluid Dynamic Effects at Speeds From M = 11 to 15. Jour. Aero. Sci., vol. 23, no. 2, Feb. 1956, pp. 108-116, 145.

4. Mueller, James N.: Conversion of Inviscid Normal-Force Coefficients in Helium to Equivalent Coefficients in Air for Simple Shapes at Hypersonic Speeds. NACA TN 3907, 1956.

5. Hammitt, A. G., and Bogdonoff, S. M.: Hypersonic Studies of the Leading Edge Effect on the Flow Over a Flat Plate. Jet Propulsion, vol. 26, no. 4, Apr. 1956, pp. 241-246, 250.

6. Munson, Albert G.: A Preliminary Experimental Investigation of the Flow Over Simple Bodies of Revolution at M = 18.4 in Helium. Memo. No. 35 (Army Ord. Contract No. DA-04-495-Ord-19), GALCIT, Dec. 15, 1956.

7. Hammitt, Andrew G.: The Hypersonic Viscous Effect on a Flat Plate With Finite Leading Edge. Rep. No. 378 (WADC TN 57-105), Dept. Aero. Eng., Princeton Univ., Mar. 1957.

8. Vas, I. E., Bogdonoff, S. M., and Hammitt, A. G.: An Experimental Investigation of the Flow Over Simple Two-Dimensional and Axial Symmetric Bodies at Hypersonic Speeds. Rep. No. 382 (WADC TN 57-246), Dept. Aero. Eng., Princeton Univ., June 1957.

9. Vas, Irwin E.: An Experimental Investigation of the Pressure on a Thin Flat Plate at Hypersonic Speeds. Rep. No. 377 (WADC TN 57-104, AD 118151), Dept. Aero. Eng., Princeton Univ., Mar. 1957.

10. Erickson, Wayne D.: Study of Pressure Distributions on Simple Sharp-Nosed Models at Mach Numbers From 16 to 18 in Helium Flow. NACA TN 4113, 1957.

11. Probstein, Ronald F.: Inversion of the Prandtl-Meyer Relation for Specific Heat Ratios of 5/3 and 5/4. WADC TN 56-497, ASTIA Doc. No. AD 110580 (Contract No. AF 33(616)-2798), Brown Univ., Nov. 1956.

12. Akin, S. W.: The Thermodynamic Properties of Helium. Trans. A.S.M.E., vol. 72, no. 6, Aug. 1950, pp. 751-757.

13. Mueller, James N.: Equations, Tables, and Figures for Use in the Analysis of Helium Flow at Supersonic and Hypersonic Speeds. NACA TN 4063, 1957.

14. Staff of the Gas Dynamics Lab., Princeton Univ.: Charts for Flow Parameters of Helium at Hypersonic Speeds - Mach Number 10 to 20. WADC Tech. Note 57-377, ASTIA Doc. No. AD 142310, U.S. Air Force, Nov. 1957.

15. Anon.: Helium Symposium (Anaheim, Calif.). Sponsored by Robertshaw-Fulton Controls Co., June 1957.

16. Bertram, Mitchel H., and Henderson, Arthur, Jr.: Effects of Boundary-Layer Displacement and Leading-Edge Bluntness on Pressure Distribution, Skin Friction, and Heat Transfer of Bodies at Hypersonic Speeds. NACA TN 4301, 1958.

17. Henderson, Arthur, Jr., and Johnston, Patrick J.: Fluid-Dynamic Properties of Some Simple Sharp- and Blunt-Nosed Shapes at Mach Numbers From 16 to 24 in Helium Flow. NASA MEMO 5-8-59L, 1959.

18. Bertram, Mitchel H., and Feller, William V.: A Simple Method for Determining Heat Transfer, Skin Friction, and Boundary-Layer Thickness for Hypersonic Laminar Boundary-Layer Flows in a Pressure Gradient. NASA MEMO 5-24-59L, 1959.

19. Lees, Lester: Hypersonic Flow. Fifth International Aeronautical Conference (Los Angeles, Calif., June 20-23, 1955), Inst. Aero. Sci., Inc., 1955, pp. 241-276.

20. Eggers, A. J., Jr., Syvertson, Clarence A., and Kraus, Samuel: A Study of Inviscid Flow About Airfoils at High Supersonic Speeds. NACA Rep. 1123, 1953. (Supersedes NACA TN 2646 by Eggers and Syvertson and NACA TN 2729 by Kraus.)

21. Laitone, Edmund V.: Exact and Approximate Solutions of Two-Dimensional Oblique Shock Flow. Jour. Aero. Sci., vol. 14, no. 1, Jan. 1947, pp. 25-41.

22. Cole, J. D.: Sweepback Theory for Shock Waves at Hypersonic Speeds. U.S. Air Force Project RAND Res. Memo. RM-1991 (ASTIA Doc. No. AD 144284), The RAND Corp., Oct. 2, 1957.

23. Van Dyke, Milton D.: A Study of Hypersonic Small-Disturbance Theory. NACA Rep. 1194, 1954. (Supersedes NACA TN 3173.)

24. Cole, J. D.: Newtonian Flow Theory for Slender Bodies. Jour. Aero. Sci., vol. 24, no. 6, June 1957, pp. 448-455.

25. Chernyi, G. G.: Hypersonic Flow Around a Body by an Ideal Gas. C-111, Morris D. Friedman, Inc. (Needham Heights 94, Mass.). (From Izvestia Otd. Tekh. Nauk (AN USSR), no. 6, 1957, pp. 77-85.)

26. Hayes, Wallace D.: Some Aspects of Hypersonic Flow. The Ramo-Wooldridge Corp., Jan. 4, 1955.

27. Li, Ting-Yi, and Geiger, Richard E.: Stagnation Point of a Blunt Body in Hypersonic Flow. Jour. Aero. Sci., vol. 24, no. 1, Jan. 1957, pp. 25-32.

28. Truitt, Robert Wesley: Hypersonic Aerodynamics. The Ronald Press Co., c.1959, pp. 253-255.

29. Serbin, H.: Hypersonic, Non-Viscous Flow Around a Circular Disk Normal to the Stream. U.S. Air Force Project RAND Res. Mem. RM-1713, The RAND Corp., May 3, 1956.

30. Freeman, N. C.: On the Theory of Hypersonic Flow Past Plane and Axially Symmetric Bluff Bodies. Jour. Fluid Mech., vol. 1, pt. 4, Oct. 1956, pp. 366-387.

31. Probstein, R. F.: Inviscid Flow in the Stagnation Point Region of Very Blunt-Nosed Bodies at Hypersonic Speeds. WADC TN 56-395 (Contract No. AF 33(616)-2798), U.S. Air Force, Sept. 1956. (Available from ASTIA as Doc. No. AD 97273.)

32. Sibulkin, Merwin: Estimation of Turbulent Heat Transfer at the Sonic Point of a Blunt-Nosed Body. Jet Propulsion, vol. 28, no. 8 pt. 1, Aug. 1958, pp. 548-554.

33. Ferri, Antonio, and Bloom, Martin H.: Cooling by Jets Directed Upstream in Hypersonic Flow. WADC Tech. Note 56-382, ASTIA Doc. No. AD-97232, U.S. Air Force, Sept. 1957.

34. Cheng, H. K., and Pallone, A. J.: Inviscid Leading-Edge Effect in Hypersonic Flow. Jour. Aero. Sci. (Readers' Forum), vol. 23, no. 7, July 1956, pp. 700-702.

35. Bertram, M. H., and Baradell, D. L.: A Note on the Sonic-Wedge Leading-Edge Approximation in Hypersonic Flow. Jour. Aero. Sci. (Readers' Forum), vol. 24, no. 8, Aug. 1957, pp. 627-628.

36. Lees, Lester, and Kubota, Toshi: Inviscid Hypersonic Flow Over Blunt-Nosed Slender Bodies. Jour. Aero. Sci., vol. 24, no. 3, Mar. 1957, pp. 195-202.

37. Liepmann, H. W., and Roshko, A.: Elements of Gas Dynamics. John Wiley & Sons, Inc., New York, 1957.

38. Dorrance, William H.: Two-Dimensional Airfoils at Moderate Hypersonic Velocities. Jour. Aero. Sci., vol. 19, no. 9, Sept. 1952, pp. 593-600.

39. Linnell, Richard D.: Two-Dimensional Airfoils in Hypersonic Flows. Jour. Aero. Sci., vol. 16, no. 1, Jan. 1949, pp. 22-30.

40. Love, Eugene S., and Grigsby, Carl E.: Some Studies of Axisymmetric Free Jets Exhausting From Sonic and Supersonic Nozzles Into Still Air and Into Supersonic Streams. NACA RM L54L31, 1955.

41. Love, Eugene S., and Lee, Louise P.: Shape of Initial Portion of Boundary of Supersonic Axisymmetric Free Jets at Large Jet Pressure Ratios. NACA TN 4195, 1958.

42. Love, Eugene S., Woodling, Mildred J., and Lee, Louise P.: Boundaries of Supersonic Axisymmetric Free Jets. NACA RM L56G18, 1956.

43. Hauser, W. C.: An Evaluation and Comparison of Methods of Predicting Skin Temperatures Due to Aerodynamic Heating. Eng. Rep. No. LB-25612, Douglas Aircraft Co., Inc., Nov. 26, 1957.

44. Rubesin, M. W., and Johnson, H. A.: A Critical Review of Skin-Friction and Heat-Transfer Solutions of the Laminar Boundary Layer of a Flat Plate. Trans. A.S.M.E., vol. 71, no. 4, May 1949.

45. Monaghan, R. J.: An Approximate Solution of the Compressible Laminar Boundary Layer on a Flat Plate. R. & M., No. 2760, British A.R.C., 1956.

46. Van Driest, E. R.: Investigation of Laminar Boundary Layer in Compressible Fluids Using the Crocco Method. NACA TN 2597, 1952.

47. Van Driest, E. R.: The Problem of Aerodynamic Heating. Aero. Eng. Rev., vol. 15, no. 10, Oct. 1956, pp. 26-41.

48. Lees, Lester, and Probstein, Ronald F.: Hypersonic Viscous Flow Over a Flat Plate. Rep. No. 195 (Contract AF 33(038)-250), Aero. Eng. Lab., Princeton Univ., Apr. 20, 1952.

49. Bertram, Mitchel H.: Boundary-Layer Displacement Effects in Air at Mach Numbers of 6.8 and 9.6. NACA TN 4133, 1958.

50. Kuo, Y. H.: Viscous Flow Along a Flat Plate Moving at High Supersonic Speeds. Jour. Aero. Sci., vol. 23, no. 2, Feb. 1956, pp. 125-136.

51. Li, Ting-Yi, and Nagamatsu, H. T.: Shock-Wave Effects on the Laminar Skin Friction of an Insulated Flat Plate at Hypersonic Speeds. Jour. Aero. Sci., vol. 20, no. 5, May 1953, pp. 345-355.

52. Lees, Lester: Influence of the Leading-Edge Shock Wave on the Laminar Boundary Layer at Hypersonic Speeds. Jour. Aero. Sci., vol. 23, no. 6, June 1956, pp. 594-600, 612.

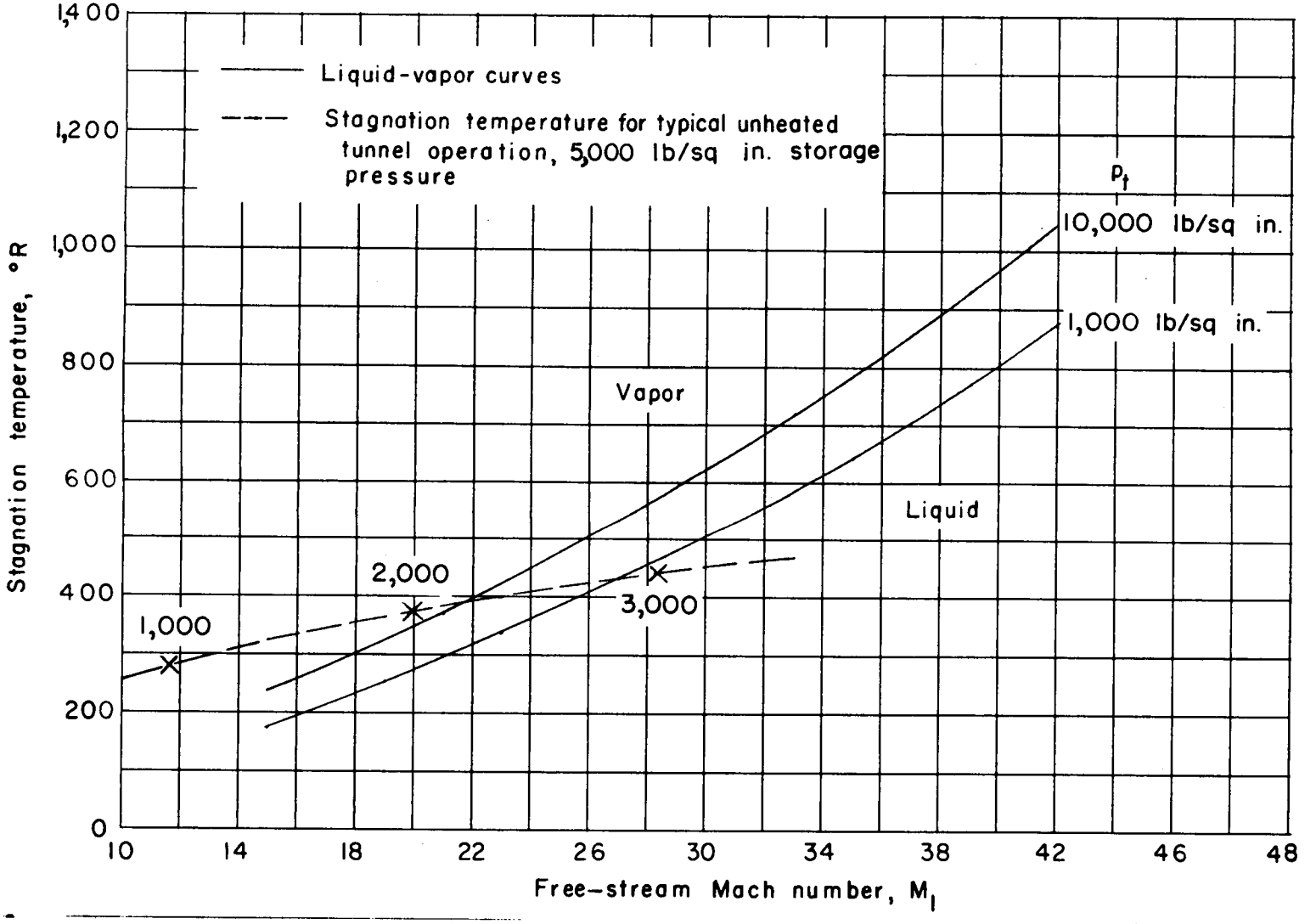

Figure 1.- Illustration of temperature requirements to avoid liquefaction in hypersonic helium tunnel. Representative values of p_t are indicated by ×.

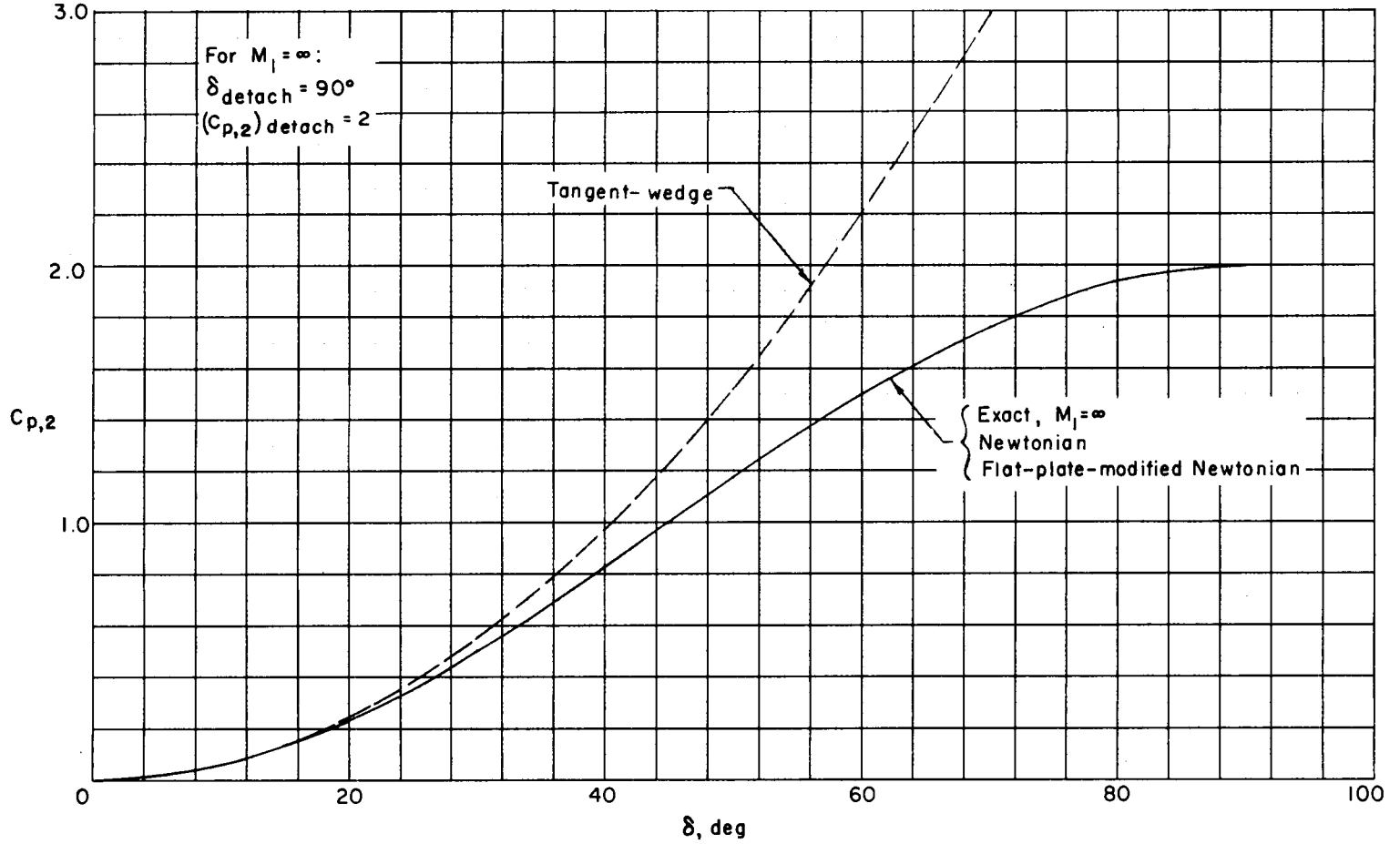

(a) $\gamma = 1.$

Figure 2.- Comparisons of several predictions of pressure coefficient on an inclined flat plate for several values of ratio of specific heats.

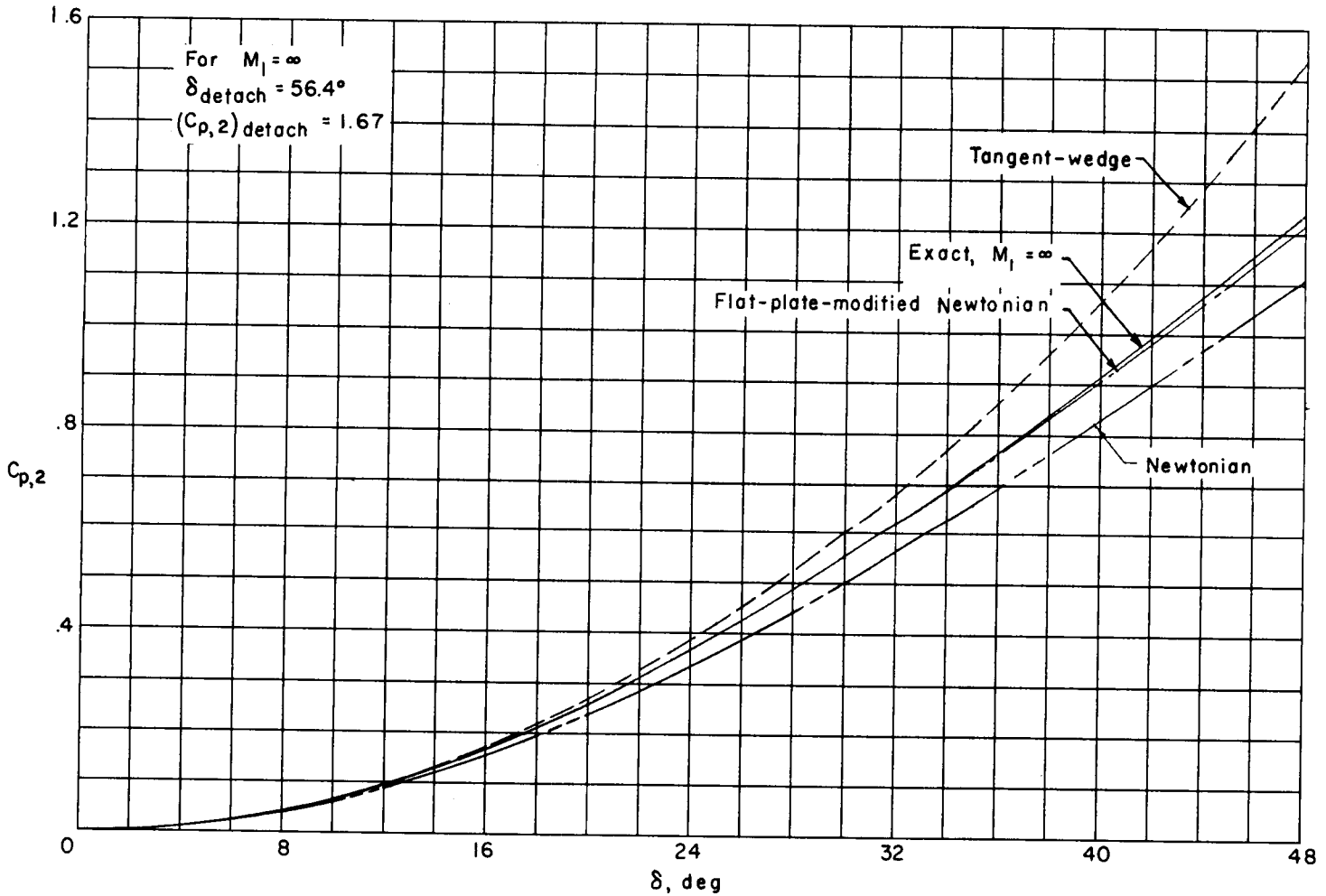

(b) $\gamma = 6/5$.

Figure 2.- Continued.

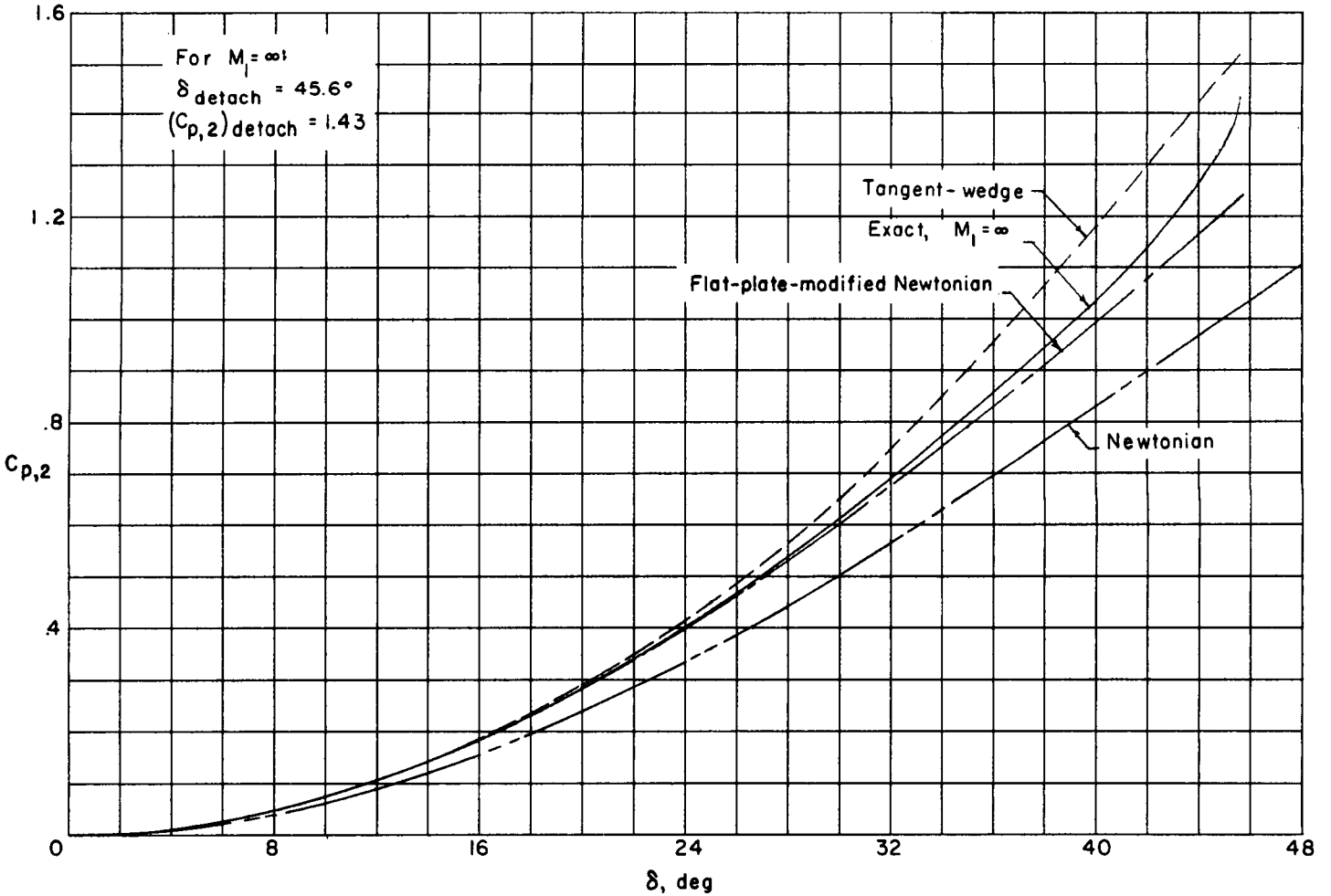

(c) $\gamma = 7/5$.

Figure 2.- Continued.

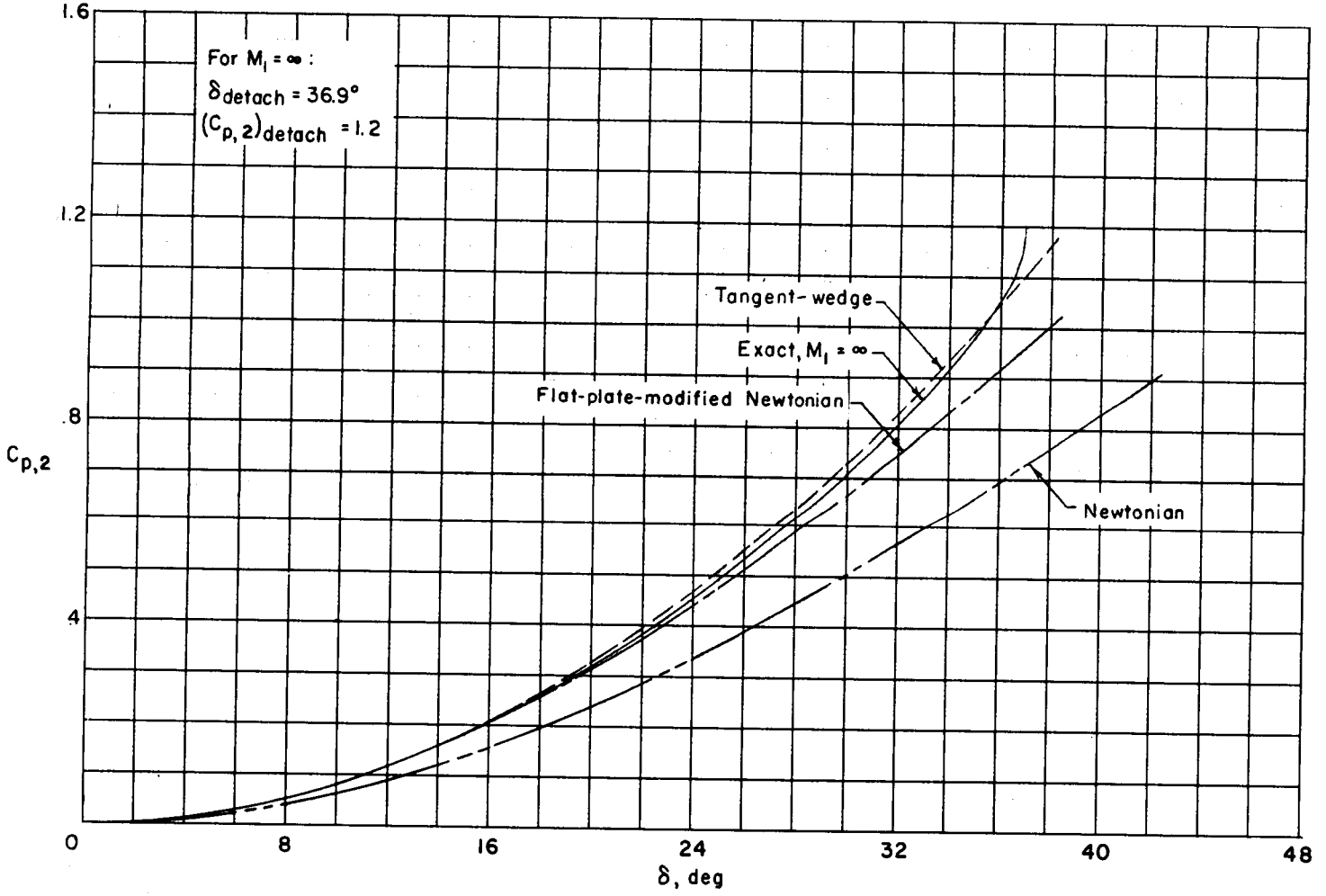

(d) $\gamma = 5/3$.

Figure 2.- Concluded.

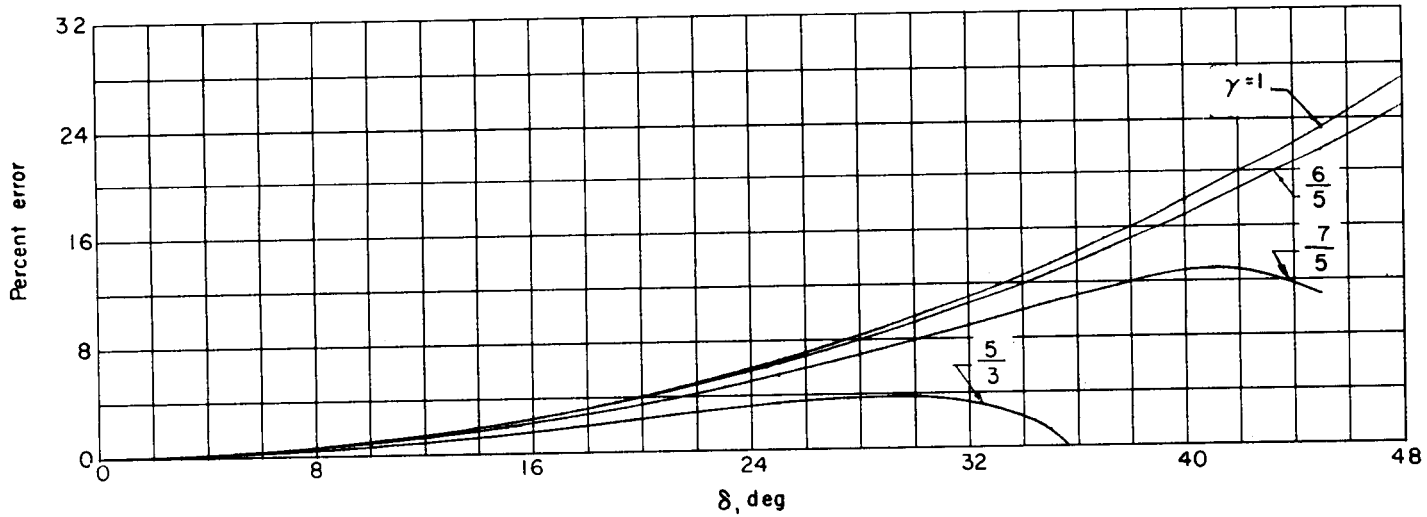

Figure 3.- Effect of ratio of specific heats upon percent error in pressure coefficient for tangent-wedge approximation at $M_1 = \infty$.

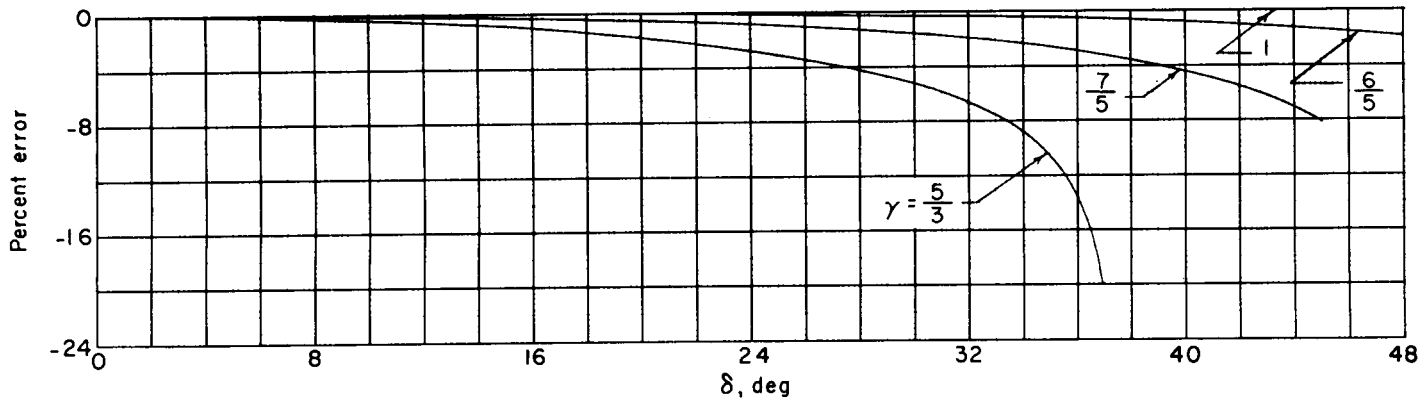

Figure 4.- Effect of ratio of specific heats upon percent error in pressure coefficient for flat-plate-modified Newtonian theory at $M_1 = \infty$.

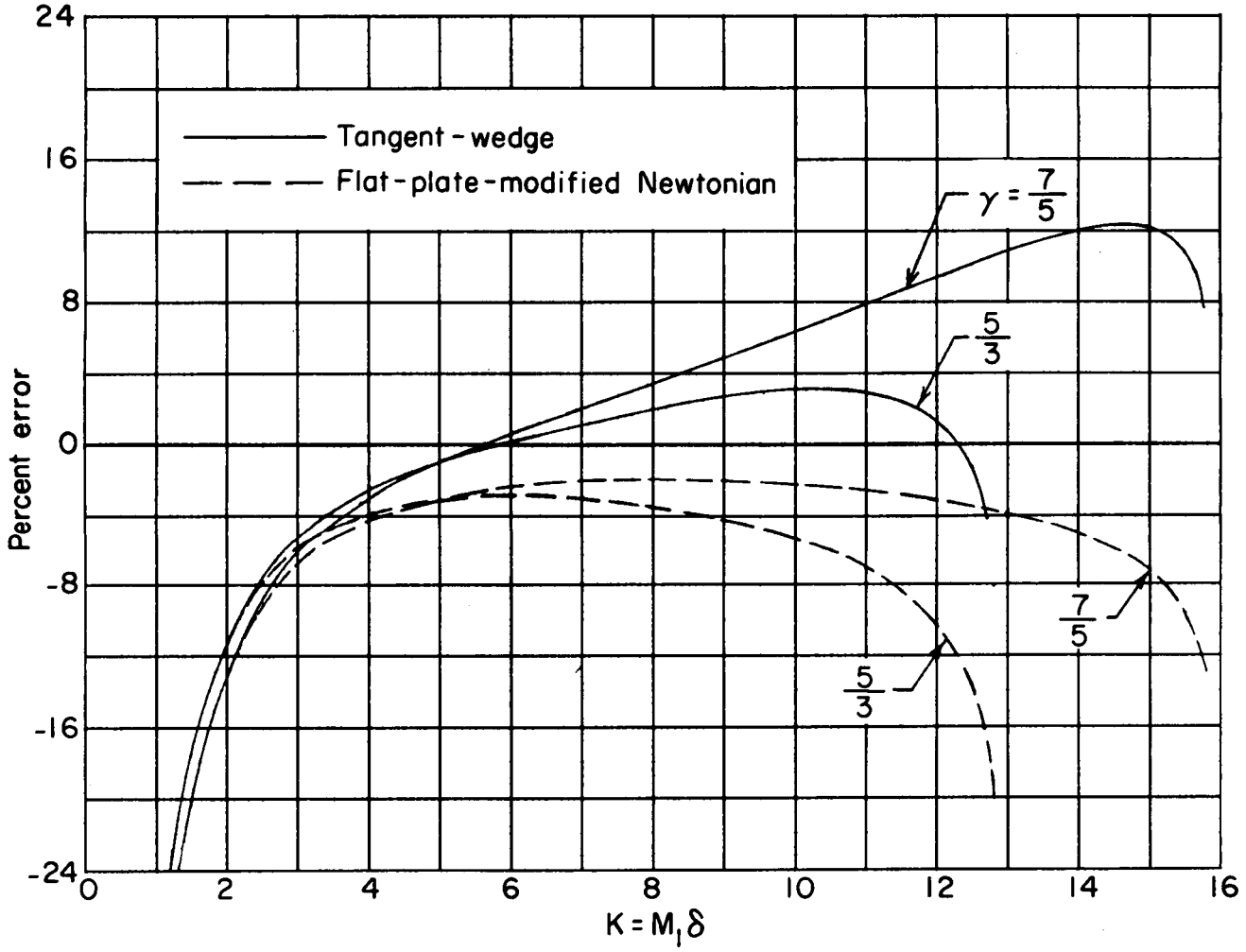

Figure 5.- Comparison of error in pressure coefficient for tangent-wedge approximation and flat-plate-modified Newtonian theory at $M_1 = 20$ in air ($\gamma = 7/5$) and in helium ($\gamma = 5/3$).

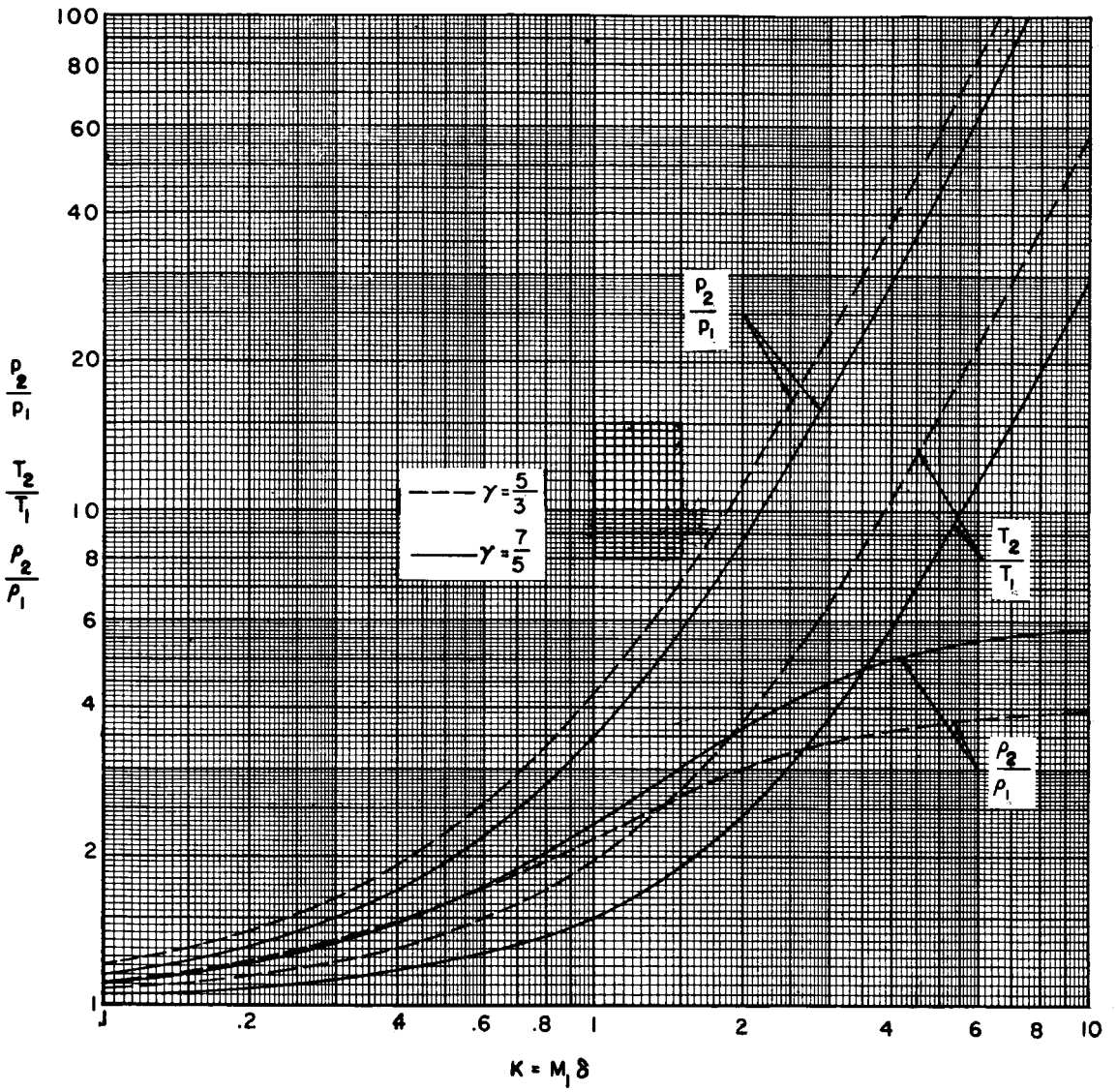

Figure 6.- Comparisons of pressure rise, temperature rise, and density rise across an oblique shock in air ($\gamma = 7/5$) and in helium ($\gamma = 5/3$) as a function of the hypersonic similarity parameter.

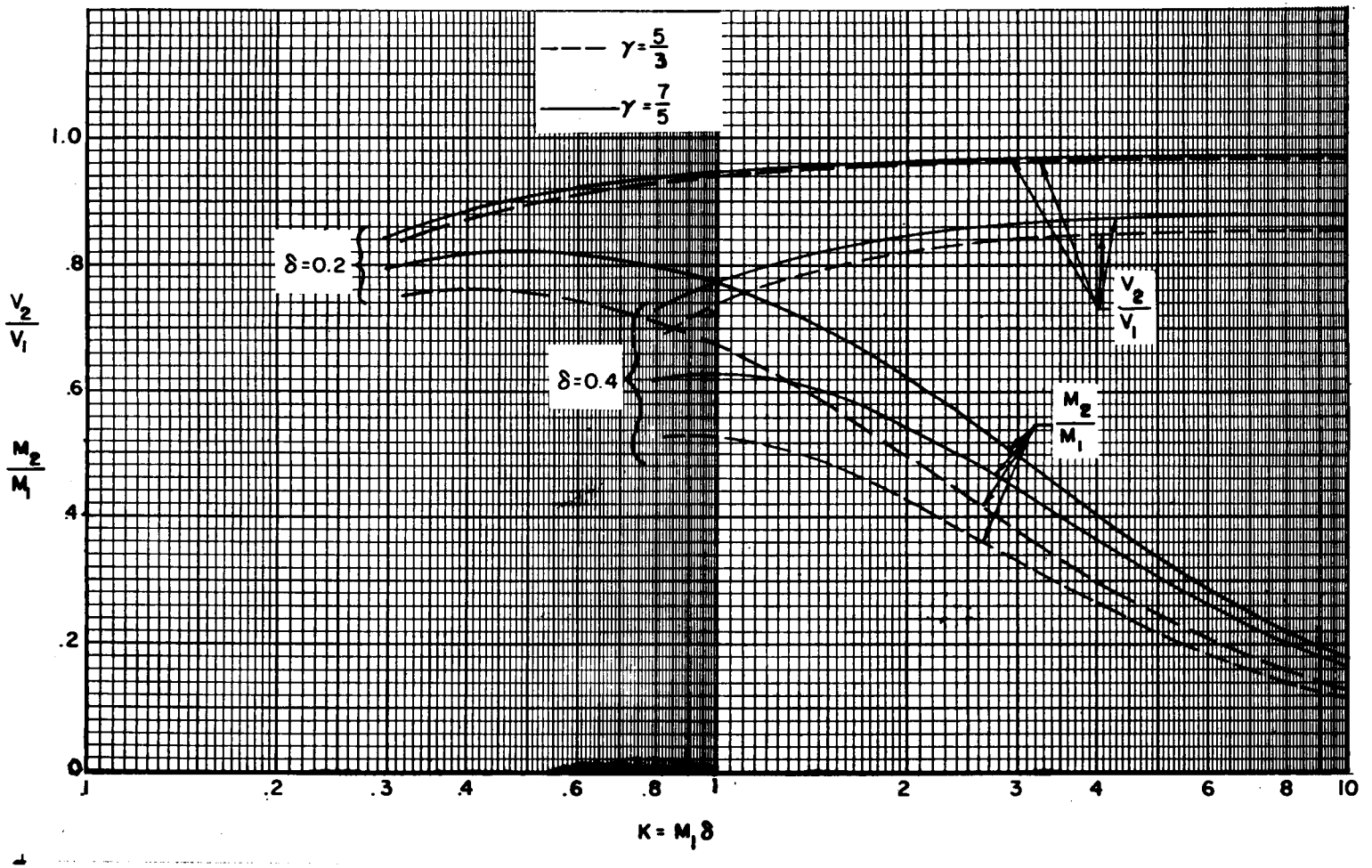

Figure 7.- Comparisons of velocity drop and Mach number drop across an oblique shock in air (γ = 7/5) and in helium (γ = 5/3) as a function of the hypersonic similarity parameter.

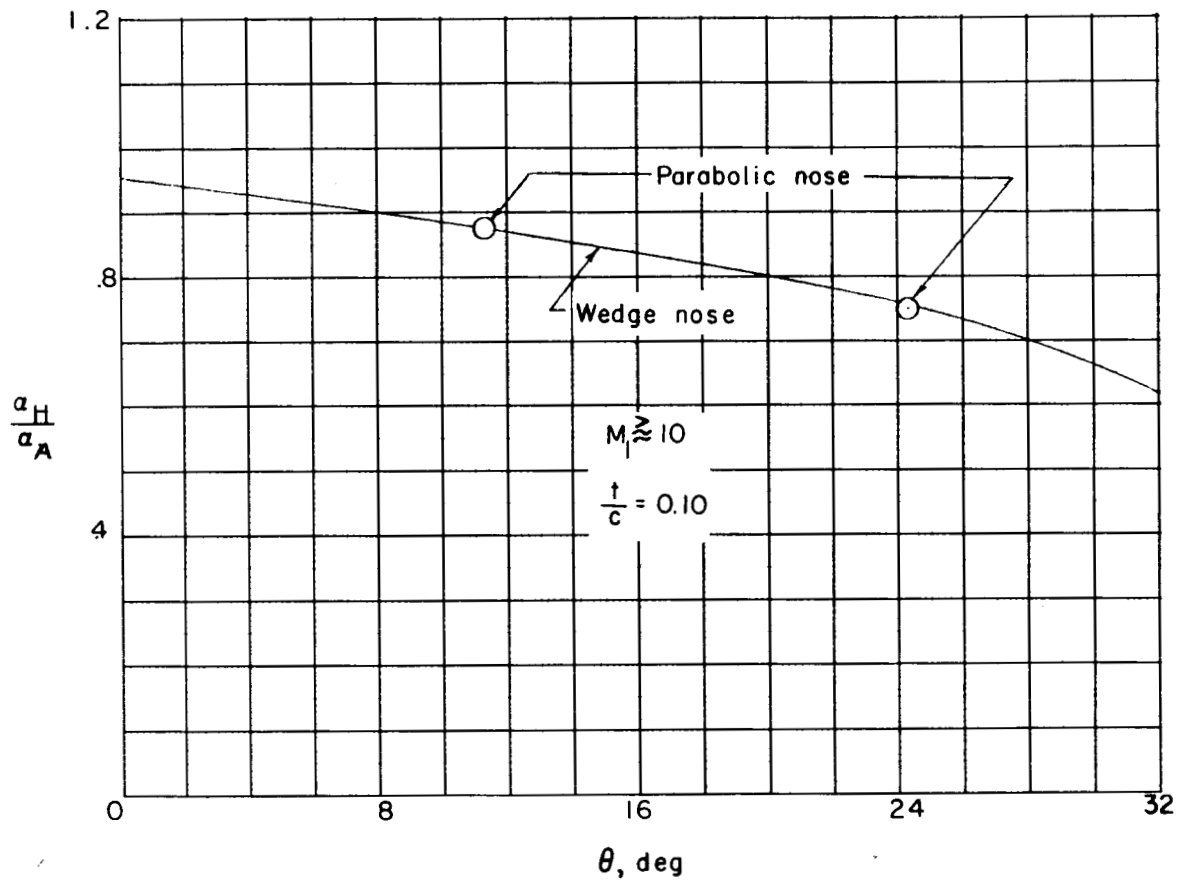

Figure 8.- Ratio of angle of attack in helium to that in air required to simulate the normal-force coefficient on inclined thick plates, with wedge and parabolic leading edges, as a function of leading-edge seminose angle (from ref. 4). $M_1 \gtrapprox 10$; $t/c = 0.10$.

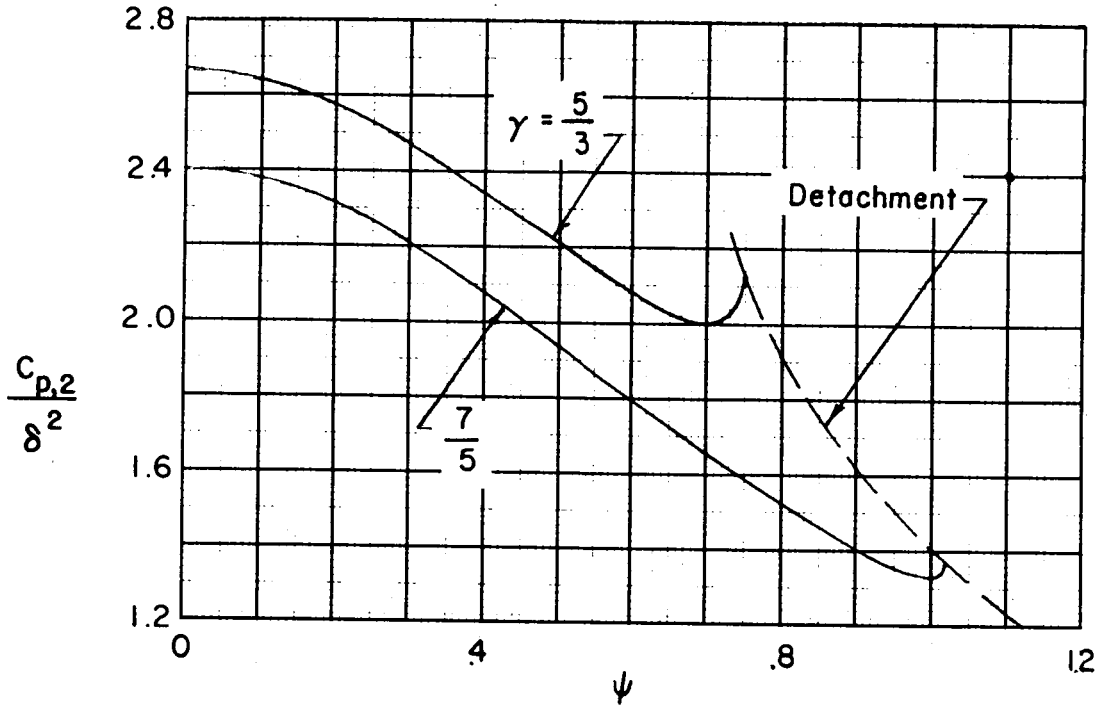

Figure 9.- Effect of flow-deflection—sweep parameter ψ on pressure coefficient for swept oblique shocks in air ($\gamma = 7/5$) and in helium ($\gamma = 5/3$) for $M_1 \to \infty$.

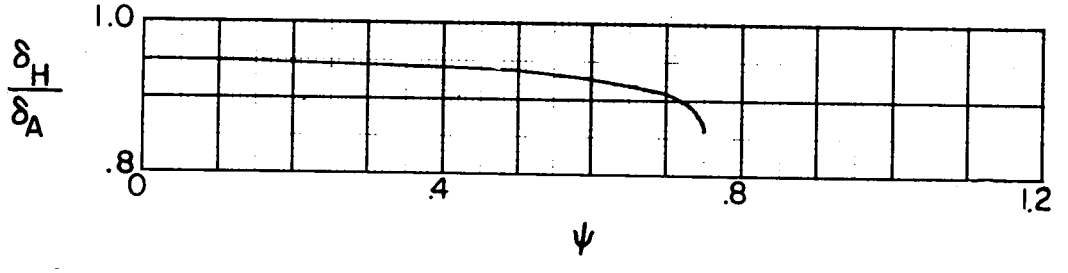

Figure 10.- Ratio of flow deflection in helium to that in air required for simulation of pressure coefficient produced by a swept oblique shock. $(C_{p,2})_H = (C_{p,2})_A$; $\psi_H = \psi_A$; $M_1 \to \infty$.

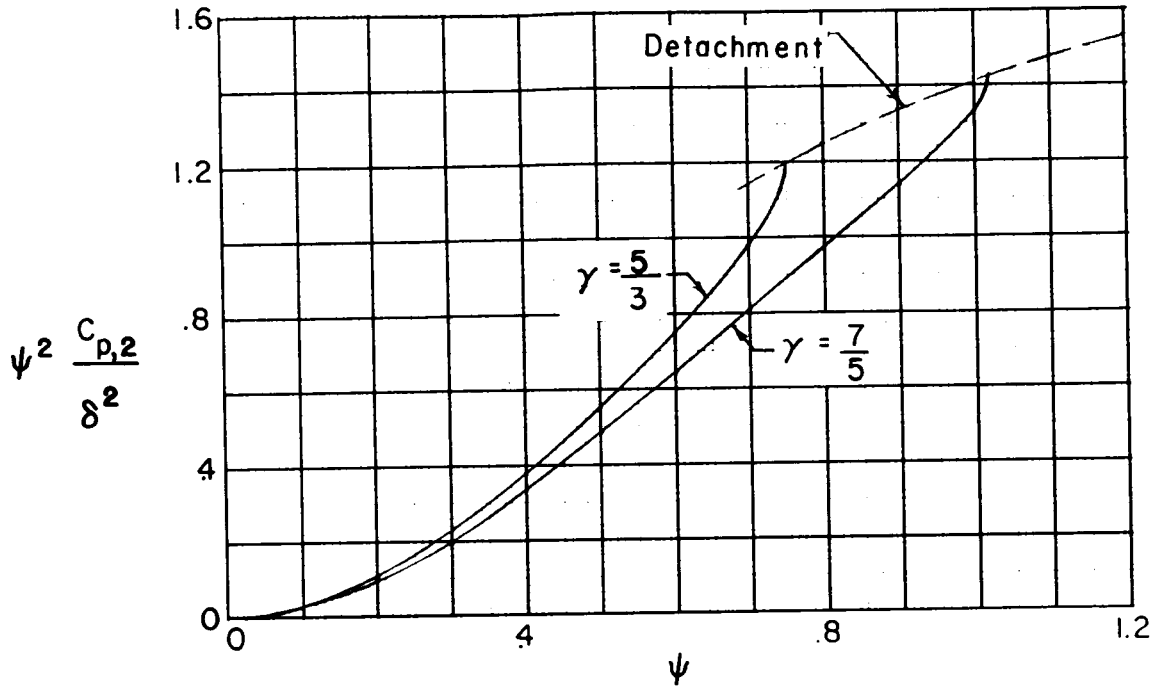

Figure 11.- Effect of the flow-deflection—sweep parameter ψ on parameter $\psi^2 \frac{C_{p,2}}{\delta^2}$ for swept oblique shocks in air ($\gamma = 7/5$) and in helium ($\gamma = 5/3$). $M_1 \to \infty$.

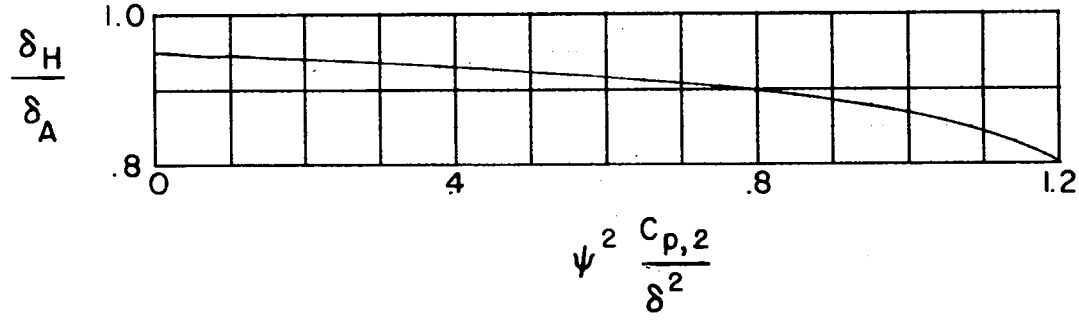

Figure 12.- Ratio of flow deflection in helium to that in air required for simulation of pressure coefficient produced by a swept oblique shock having same angle of sweepback in air and in helium.
$(C_{p,2})_H = (C_{p,2})_A$; $\Lambda_H = \Lambda_A$; $\frac{\psi_H}{\psi_A} = \frac{\delta_H}{\delta_A}$.

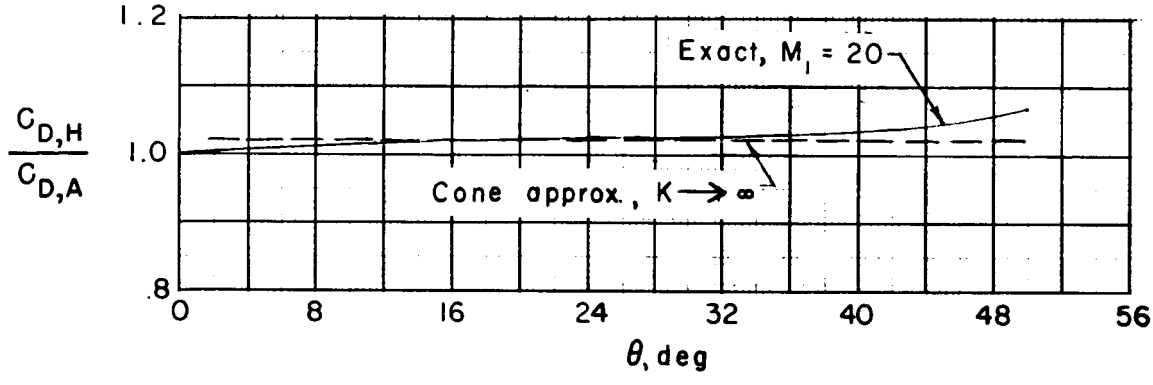

(a) Cones.

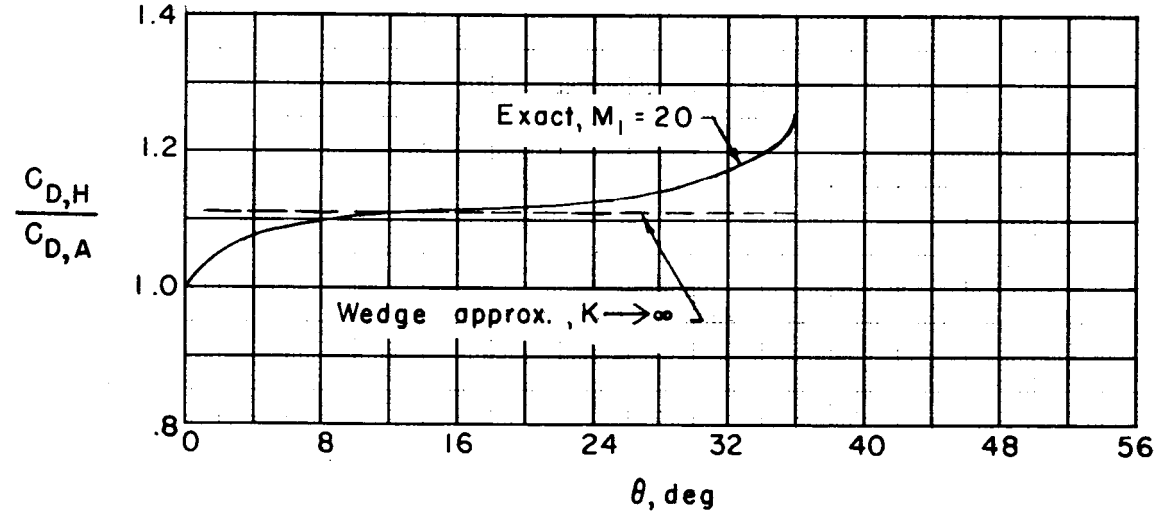

(b) Wedges.

Figure 13.- Ratio of drag coefficients of cones and wedges in helium to those in air as a function of the seminose angle.

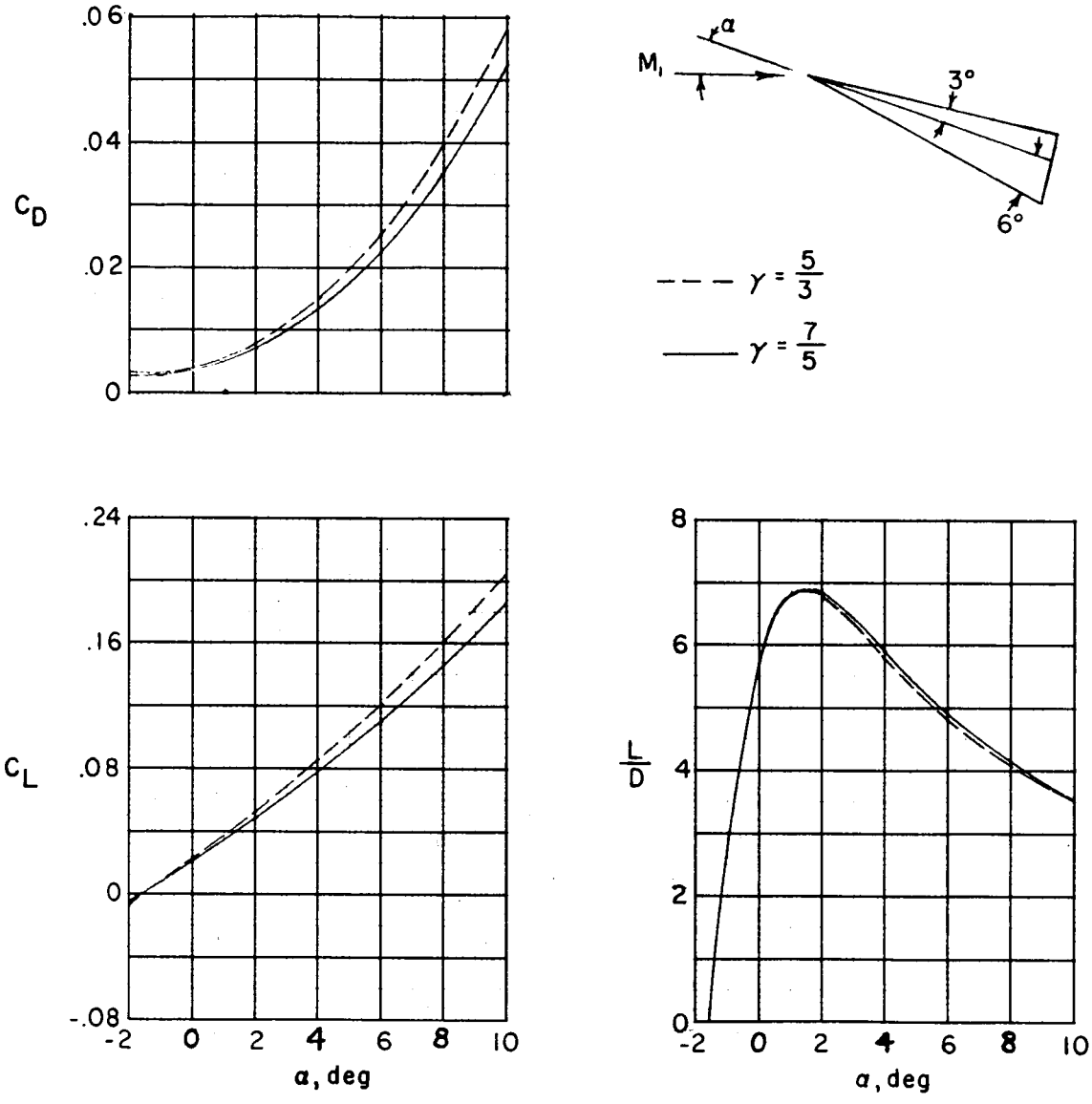

Figure 14.- Comparisons of lift and drag coefficients and lift-drag ratio of an asymmetric wedge in air (γ = 7/5) and in helium (γ = 5/3) as determined from exact calculations. Base pressure assumed equal to free-stream static pressure. M_1 = 20.

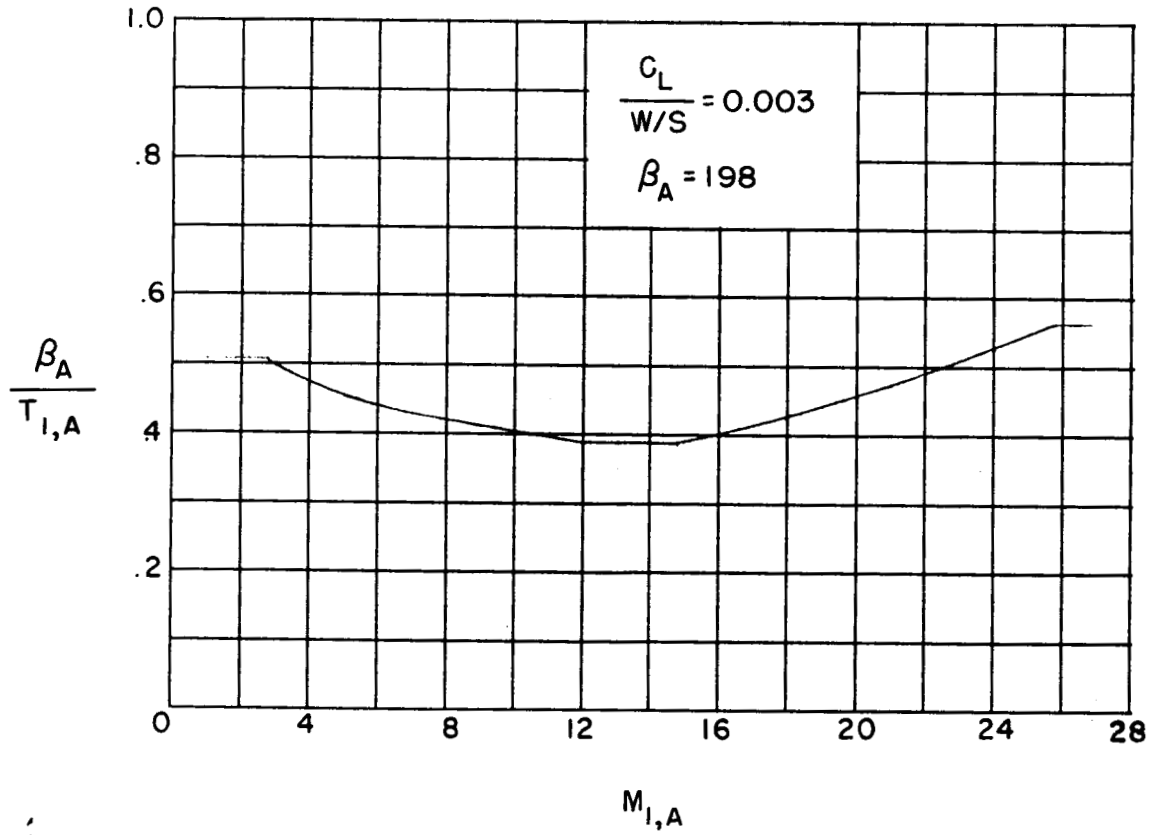

Figure 15.- Variation of $\beta_A/T_{1,A}$ with free-stream Mach number employed in flight example.

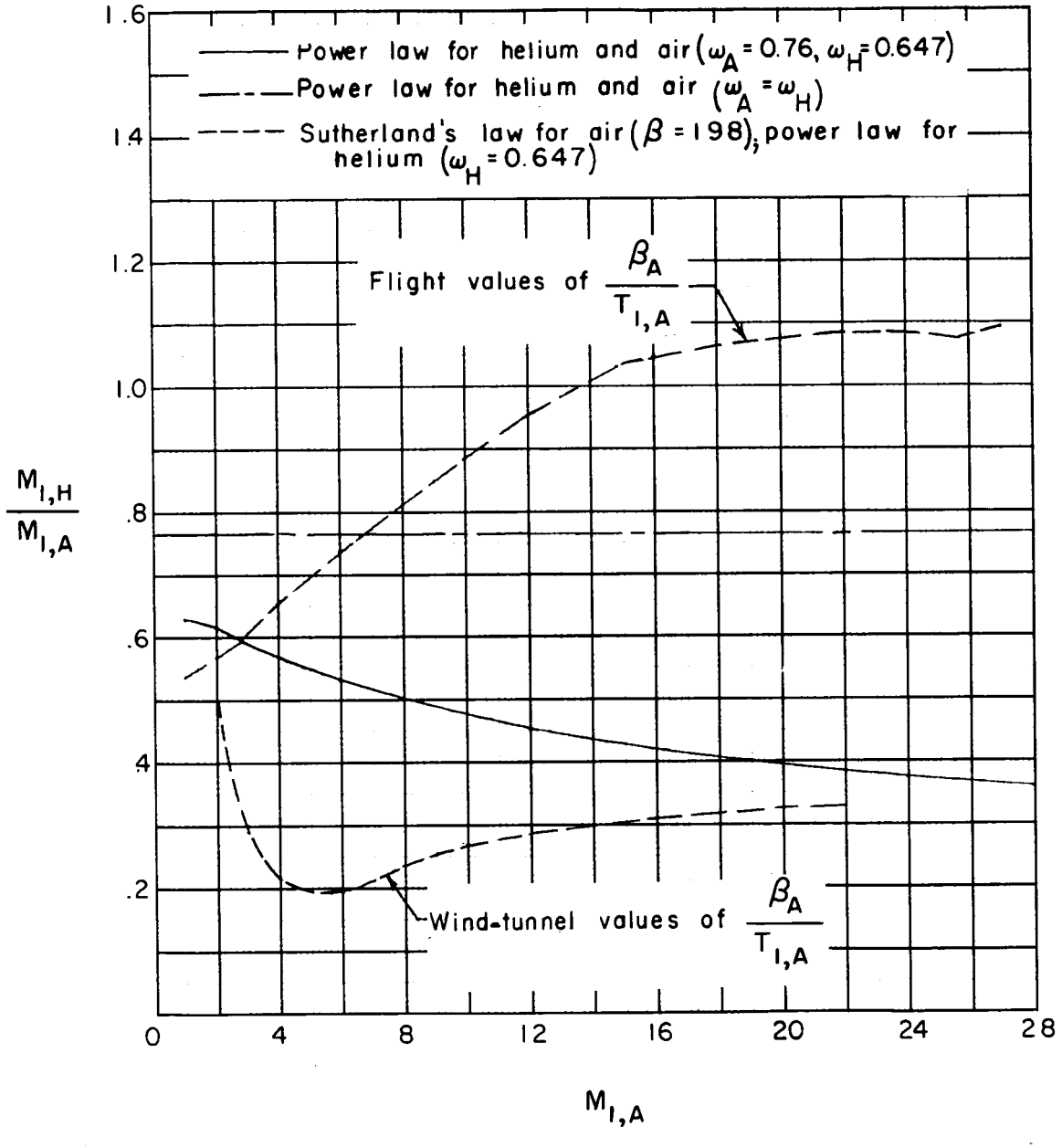

(a) Laminar flow.

Figure 16.- Ratio of free-stream Mach number in helium to that in air required for simulation of average skin-friction coefficient for laminar flow. $C_{F,H} = C_{F,A}$; $R_H = R_A$; $N_{Pr} = 1$; insulated plate.

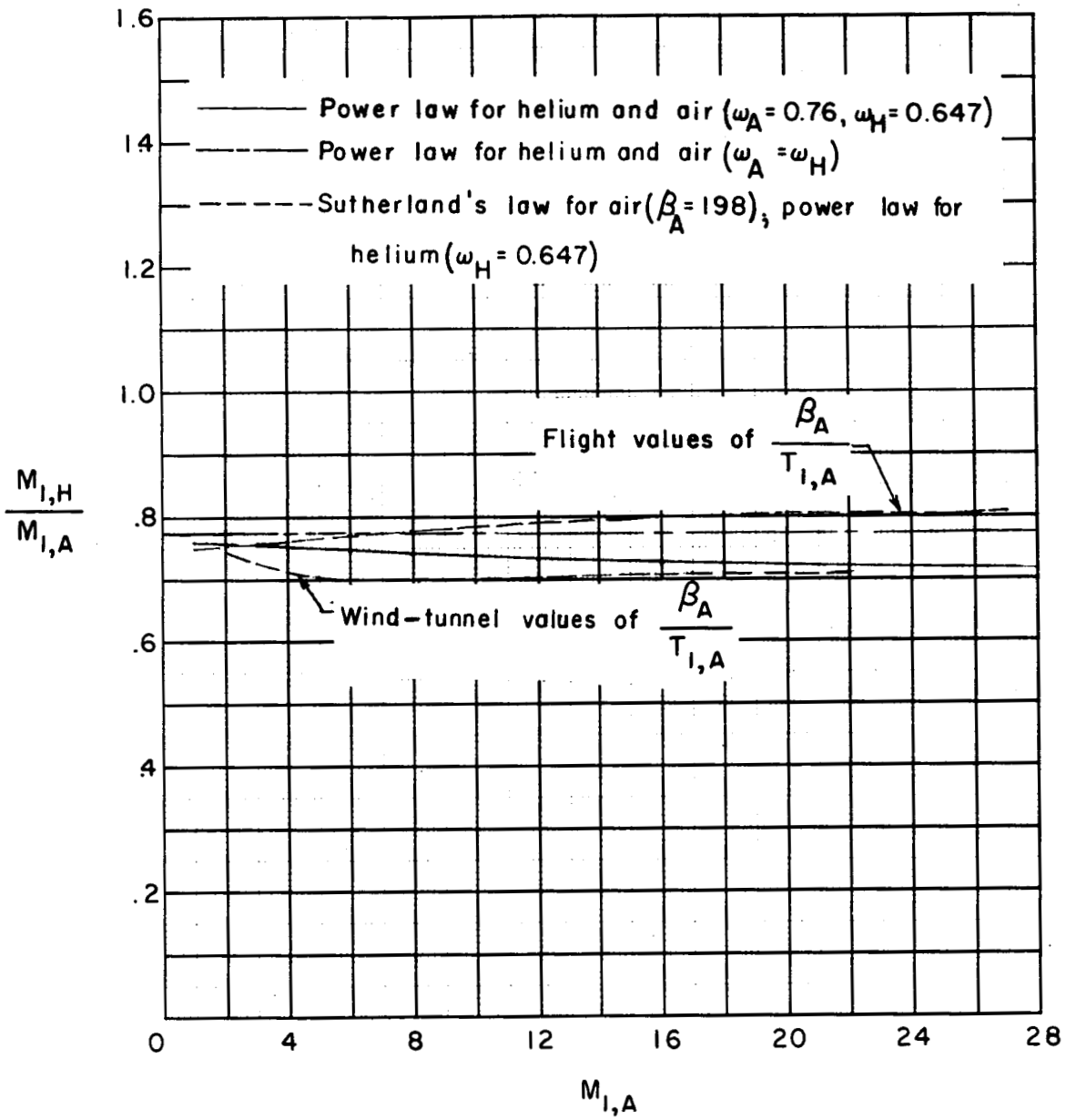

(b) Turbulent flow.

Figure 16.- Concluded.

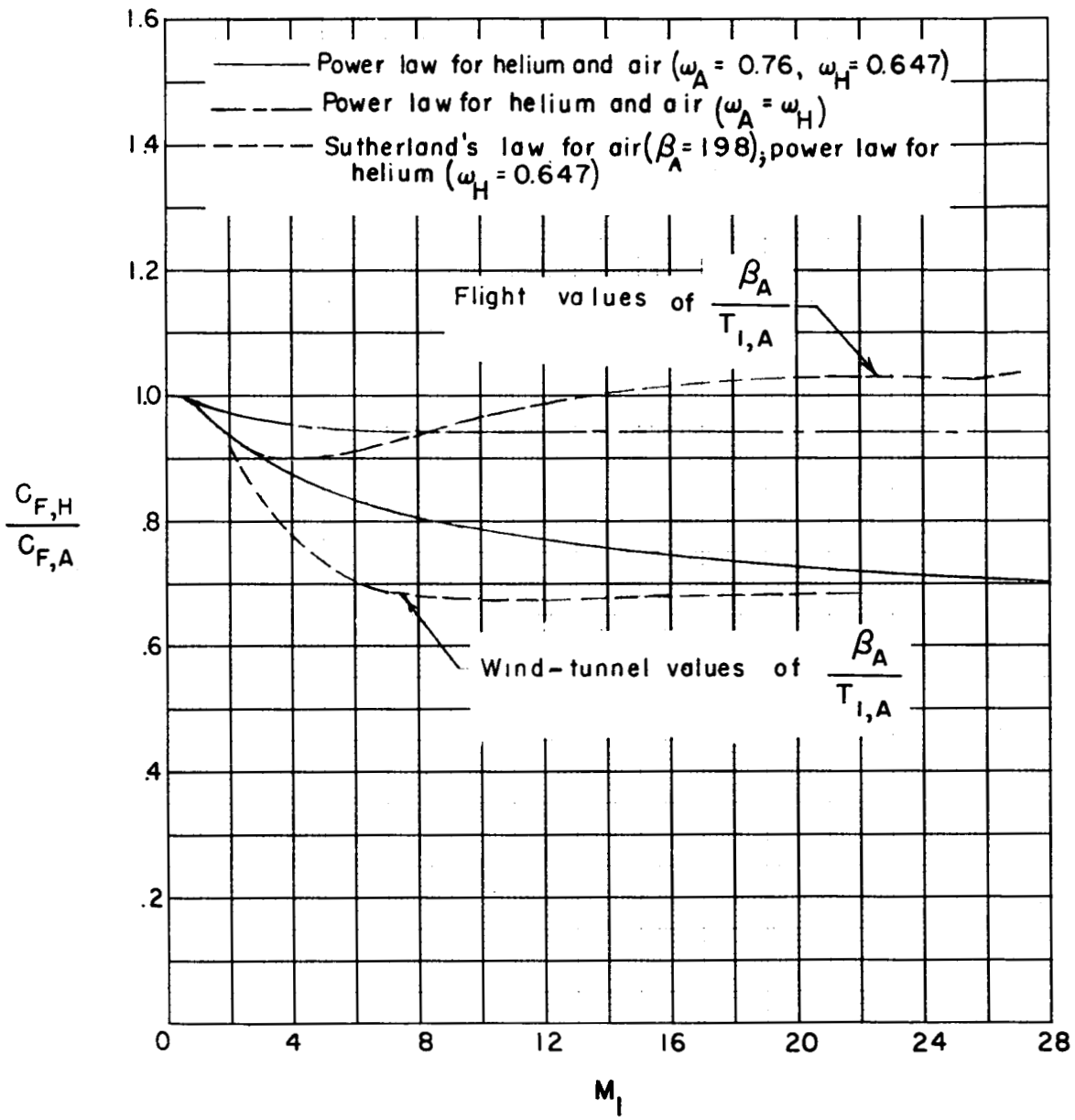

(a) Laminar flow.

Figure 17.- Ratio of average skin-friction coefficient in helium to that in air. $M_{l,H} = M_{l,A}$; $R_H = R_A$; $N_{Pr} = 1$; insulated plate.

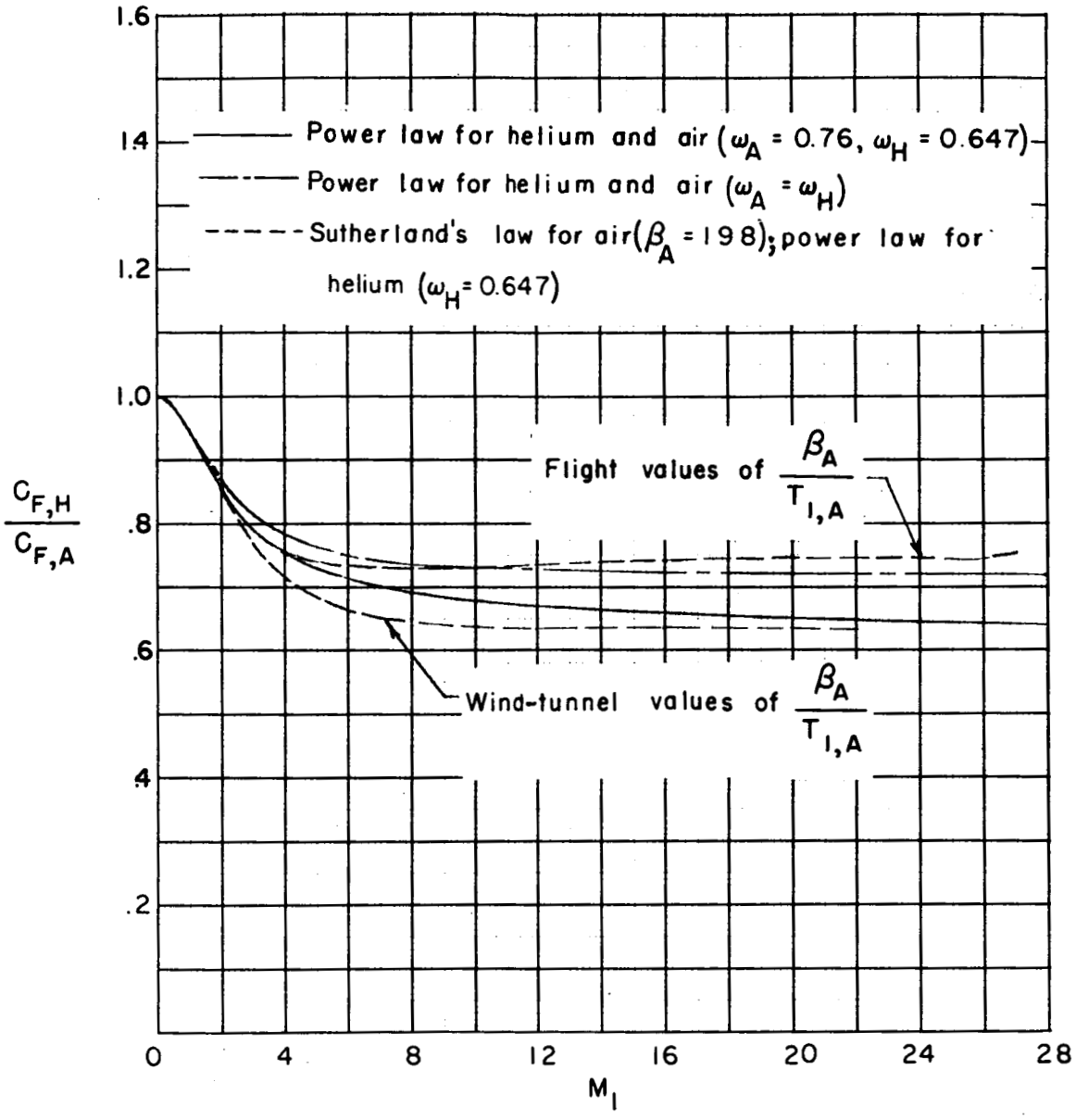

(b) Turbulent flow.

Figure 17.- Concluded.

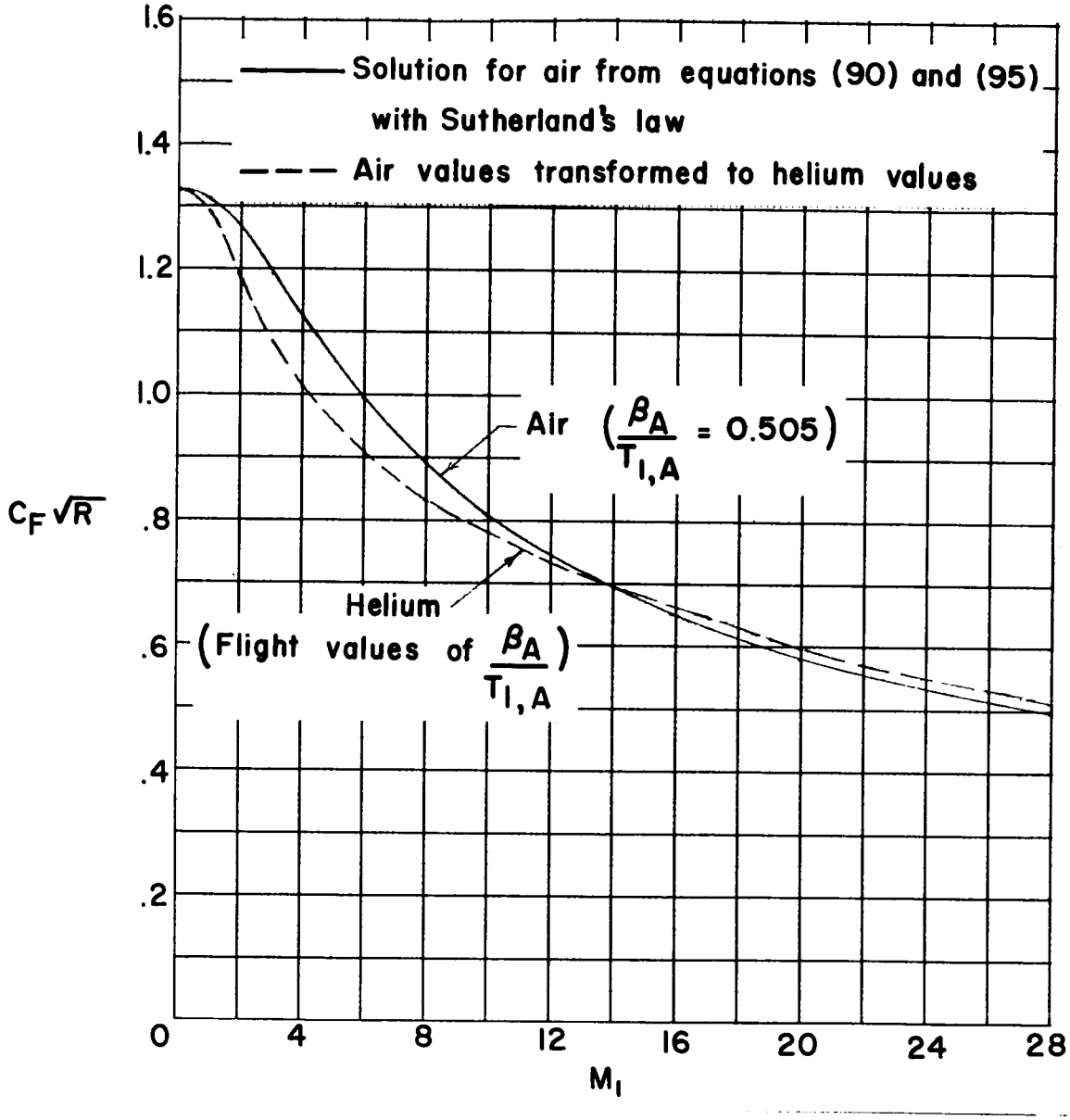

Figure 18.- Effect of Mach number on average skin-friction coefficient in air and in helium for laminar flow. $\omega_H = 0.647$; $N_{Pr} = 1$; insulated plate.

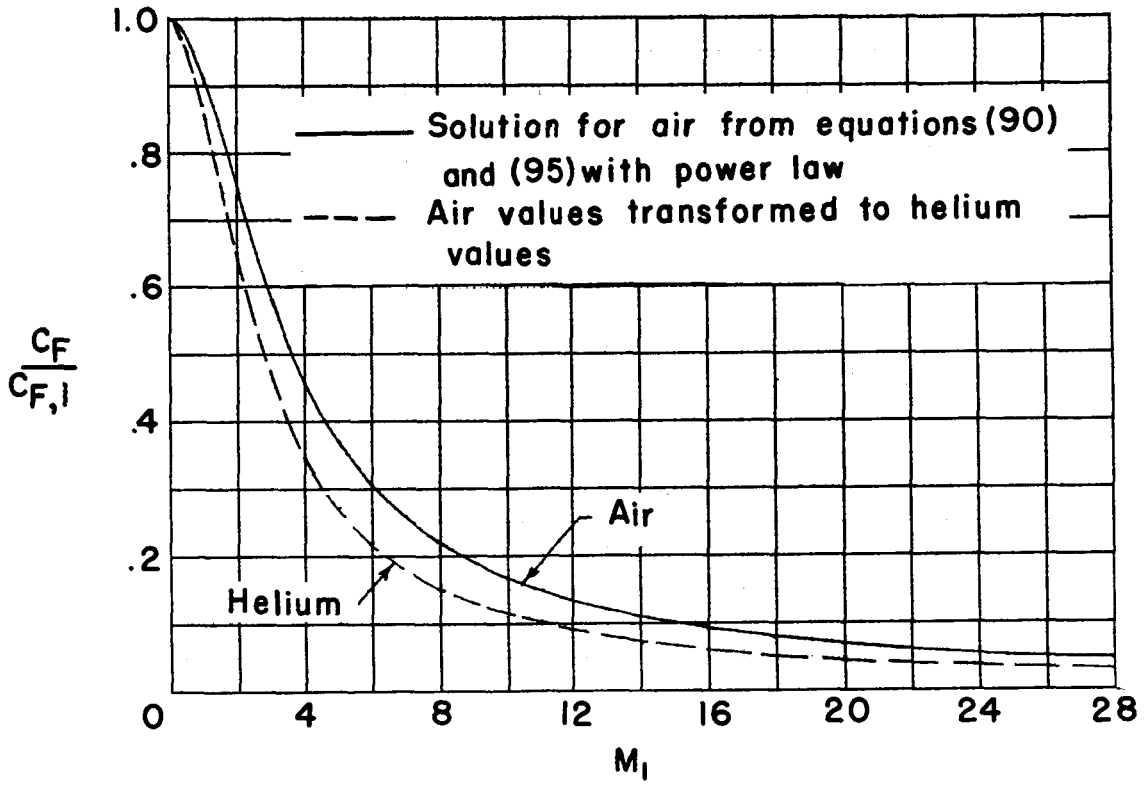

Figure 19.- Effect of Mach number on ratio of average skin-friction coefficient to incompressible skin-friction coefficient in air and in helium for turbulent flow. $\omega_A = 0.76$; $\omega_H = 0.647$; $R \approx 10^7$; $N_{Pr} = 1$; insulated plate.

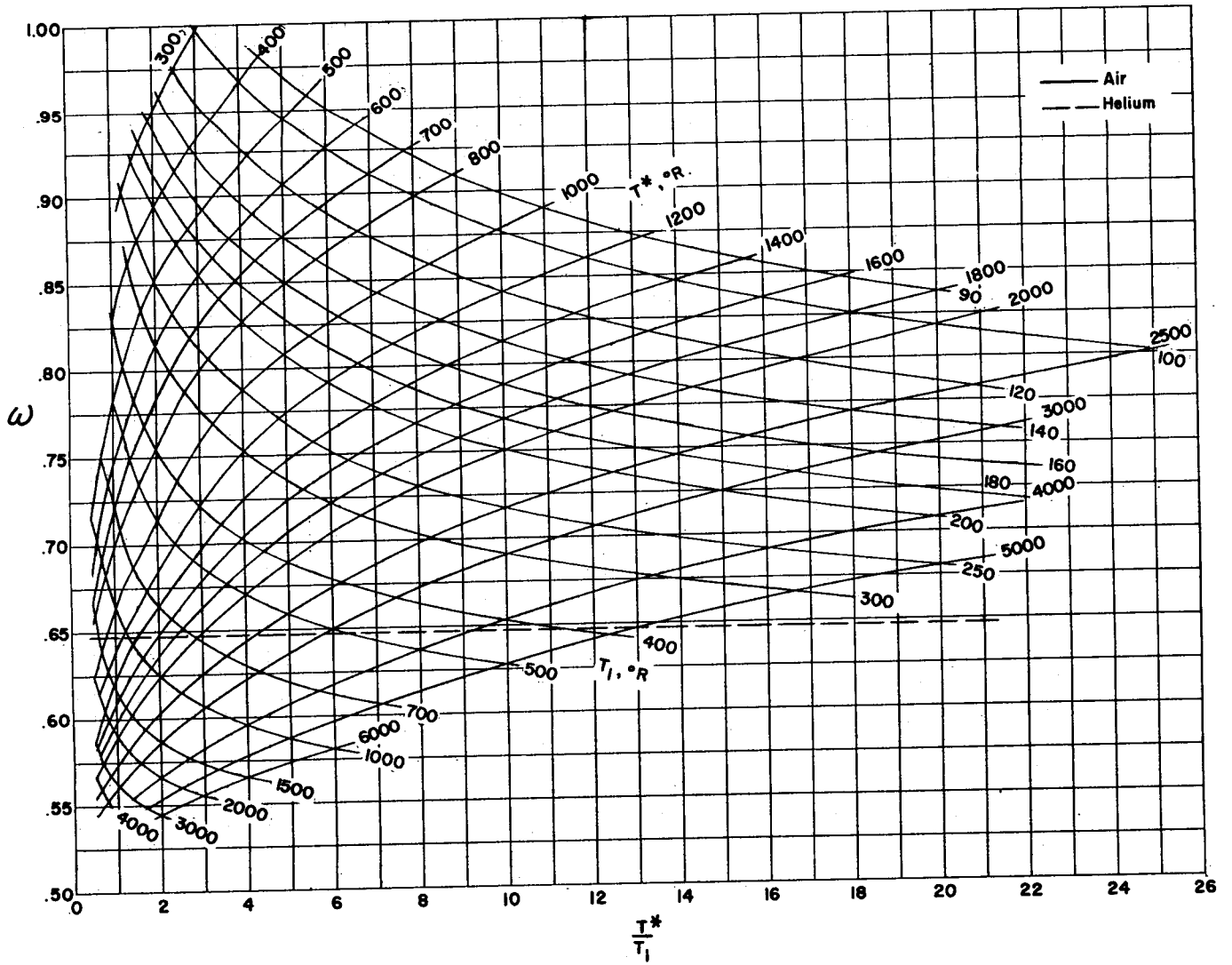

Figure 20.- Effect of temperature level and reference-temperature ratio on value of ω.